

Block Copolymer Derived Electrospun Mesoporous Nanofibers

**Akash Nathani
CH14MTECH11002**

A Dissertation Submitted to
Indian Institute of Technology Hyderabad
In Partial Fulfillment of the Requirements for
The Degree of Master of Technology



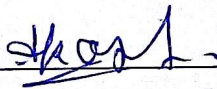
भारतीय प्रौद्योगिकी संस्थान हैदराबाद
Indian Institute of Technology Hyderabad

Department of Chemical Engineering

June, 2016

Declaration

I declare that this written submission represents my ideas in my own words, and where others' ideas or words have been included, I have adequately cited and referenced the original sources. I also declare that I have adhered to all principles of academic honesty and integrity and have not misrepresented or fabricated or falsified any idea/data/fact/source in my submission. I understand that any violation of the above will be a cause for disciplinary action by the Institute and can also evoke penal action from the sources that have thus not been properly cited, or from whom proper permission has not been taken when needed.



(Signature)

Akash Nathani
CH14MTECH11002

Approval Sheet

This thesis entitled “**Block Copolymer Derived Electrospun Mesoporous Nanofibers**” by Akash Nathani (CH14MTECH11002) is approved for the degree of Master of Technology from IIT Hyderabad.

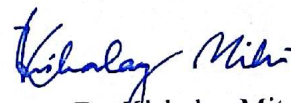


Dr. Mudrika Khandelwal

Department of Material Science and
Metallurgical Engineering

Indian Institute of Technology Hyderabad

Examiner



Dr. Kishalay Mitra

Department of Chemical Engineering

Indian Institute of Technology Hyderabad

Examiner



Dr. Saptarshi Majumdar

Department of Chemical Engineering

Indian Institute of Technology Hyderabad

Examiner



Dr. Chandra Shekhar Sharma

Department of Chemical Engineering

Indian Institute of Technology Hyderabad

Advisor

Acknowledgements

First I would like to thank my supervisor **Dr. Chandra Shekhar Sharma** for his support and guidance throughout this work.

My sincere thanks to my thesis committee members **Dr. Saptarshi Majumdar**, **Dr. Mudrika Khandelwal** and **Dr. Kishalay Mitra** for their encouragement, time and suggestions.

I would also like to thank my lab mates Ramya Araga for helping me with FTIR and pyrolysis process, Kali Suresh for his help in FESEM and TEM characterization, Dr. Manohar Kakunuri for his suggestions, Srinadh Mattaparthi for his help in contact angle measurements and Suresh Mamidi for his help in pyrolysis process.

Abstract

In this study we have successfully demonstrated the synthesis of porous polymer/polymer derived carbon nanofibers from two block copolymer systems. In first case poly(styrene-block-methylmethacrylate) (PS-b-PMMA) of three different molecular weights were used to produce nanofibers with different morphologies. Various electrospinning parameters such as applied potential difference, distance between spinneret and collector, flowrate and the concentration of polymer in an organic solvent were optimized to get fine fibers. Fibers thus obtained were annealed to undergo a microphase separation followed by UV exposure treatment which causes crosslinking of one phase and at the same time degradation of another phase. The degraded phase was then etched out using a weak acid to obtain the desired porosity. The porous fibers thus obtained were characterized using field emission electron microscopy (FESEM) and fourier transmission infrared spectroscopy (FTIR). Wettability studies were also carried out for the different morphologies. In second case a blend of a homopolymer (polyacrylonitrile (PAN)) and a copolymer (poly(acrylonitrile-block-methylmethacrylate) (PAN-b-PMMA)) was electrospun. The similar protocol was followed to achieve the porosity as mentioned above. The porous fibers thus obtained were carbonized and followed by characterization using FESEM, FTIR, Transmission electron microscopy (TEM) and Raman spectroscopy. Further a data based modeling of electrospun PAN fibers was also carried out to predict the morphology of the fibers. For this purpose, a sufficiently large dataset was created by varying the above mentioned electrospinning parameters.

Nomenclature

nm	Nanometer
PS-b-PMMA	Polystyrene-b-poly(methylmethacrylate)
PEG-b-PS	Polyethylene glycol-b-polystyrene
PS-b-PPG	Polystyrene-b-polypropylene glycol
DMF	Dimethylformamide
PLGA	Poly(lactide-co-glycolide)
PEG-b-PCL	Polyethylene-b-polycaprolactone
SEM	Scanning Electron Microscope
BCP	Block copolymer
THF	Tetrahydrofuran
M _w	Weight molecular average
M _n	Number molecular average
UV	Ultraviolet
FTIR	Fourier Transform Infrared Radiation
TGA	Thermogravimetric analysis
SDFCL	S D Fine-Chem Limited
ml	Milliliter
kV	Kilovolts
μl	Microliter
cm	Centimeter
DI	De-ionized (water)
mm	Millimeter
χ_{AB}	Interaction parameter
γ_{SG}	Interfacial tension between solid and liquid medium
γ_{LG}	Interfacial tension between liquid and vapor medium
γ_{SL}	Interfacial tension between solid and vapor medium
cos θ	Contact angle
PAN	Polyacrylonitrile
PAN-b-PMMA	Polyacrylonitrile-b-poly(methylmethacrylate)

Contents

1 Introduction	
1.1 Nanofibers	1
1.1.1 Drawing.....	1-2
1.1.2 Template Synthesis.....	2
1.1.3 Phase Separation.....	3
1.1.4 Self-Assembly.....	4
1.1.5 Electrospinning.....	5-9
1.2 Block Co-polymers	9-12
1.3 Objective and Layout.....	12-15
2 Mesoporous Nanofibers prepared by Solution Electrospinning of PS-b-PMMA	
2.1 Materials.....	16-17
2.2 Method	17-21
2.2.1 Preparation of solution	17
2.2.2 Electrospinning.....	18-20
2.2.3 Formation of porous PS-b-PMMA fibers.....	21
2.3 Characterization and Analysis.....	21-36
2.3.1 Characterization using SEM	21-31
2.3.2 FTIR	31-33
2.3.3 Wettability Studies.....	33-36
3 PAN-b-PMMA Derived Electrospun Nanofibers	
3.1 Materials	37
3.2 Method	37-40
3.2.1 Preparation of solution.....	37
3.2.2 Electrospinning.....	37-38
3.2.3 Formation of porous PAN-b-PMMA fibers.....	38-39
3.2.4 Carbonization.....	39-40
3.3 Characterization and Analysis	40-44
3.3.1 FTIR	40-42
3.3.2 Raman spectroscopy	42-43
3.3.3 Transmission electron microscopy.....	43-44

4 Data based modeling of electrospun PAN nanofibers	
4.1 Materials	45
4.2 Experimentation	45
4.3 Characterization	45-46
5 Summary and Future Work	47-48
References	49-50

Chapter 1

Introduction

1.1 Nanofibers

The fibers with a diameter less than 1000 nm are termed as nanofibers. Nanofibers are classified under the category of 1D nanomaterials, as two of its dimensions lie in the 'Nano' range. Due to its unique properties such as large specific surface area, high mechanical strength and ease of surface functionalization, nanofibers are seen as an attractive material for application in catalysis, sensing, protective clothing, filtration, tissue engineering scaffolds and nano-electronics [1] [2].

The strategies for the synthesis of nanofibers can be broadly classified into two categories, the top-down approach, and the bottom-up approach. A number of techniques for synthesis of nanofibers have been developed recently, they include template synthesis drawing, self-assembly, phase separation, magnetospinning, and electrospinning.

1.1.1 Drawing

In this process, a micropipette is dipped into a polymer droplet using a micromanipulator. The micropipette is then withdrawn from the droplet and moved back at a slow speed of about 10^{-4} m/s, resulting into pulling out of a nanofiber. The fiber is then deposited on a surface by touching it with the end of the micropipette [1].

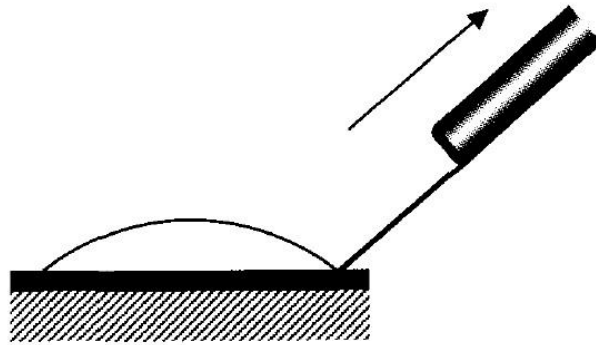


Fig 1.1: Schematic of drawing process [1]

1.1.2 Template Synthesis:

In this process, a templet or a mold is used to synthesize nanofibers. Templet may be a metal oxide membrane with pores of nanoscale dimensions. The polymer is extruded from this membrane by applying pressure from one side of the membrane, water is used as media for application of this pressure. Another side of the membrane consists of a solidifying solution which assists in the formation of fibers. The diameter of fibers thus obtained is dictated by the pore size of the membrane [1].

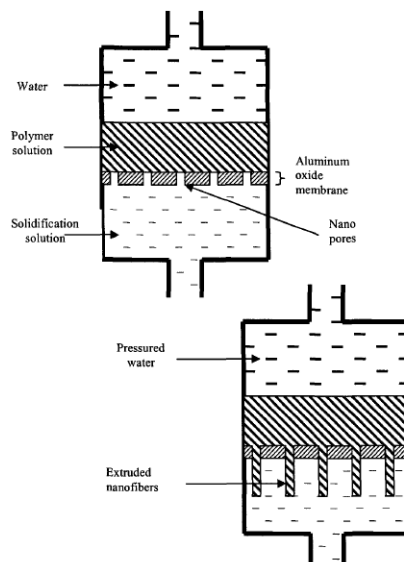


Fig 1.2: Schematic of template synthesis process [1].

1.1.3 Phase Separation

This technique, as the name suggest, is on the phase separation of two incompatible phases. Fibers are produced in a series of steps, which include polymer dissolution, gelation, solvent extraction, freezing and freeze-drying.

Initially a solution of the desired polymer is made with the suitable solvent, and then this solution is transferred to a refrigerator which is set to gelation temperature. Distilled water is added to the formed gel thus formed for solvent exchange to take place and this water is changed multiple times. Later it is refrigerated again followed by freeze drying to obtained the polymer fibers. [1]

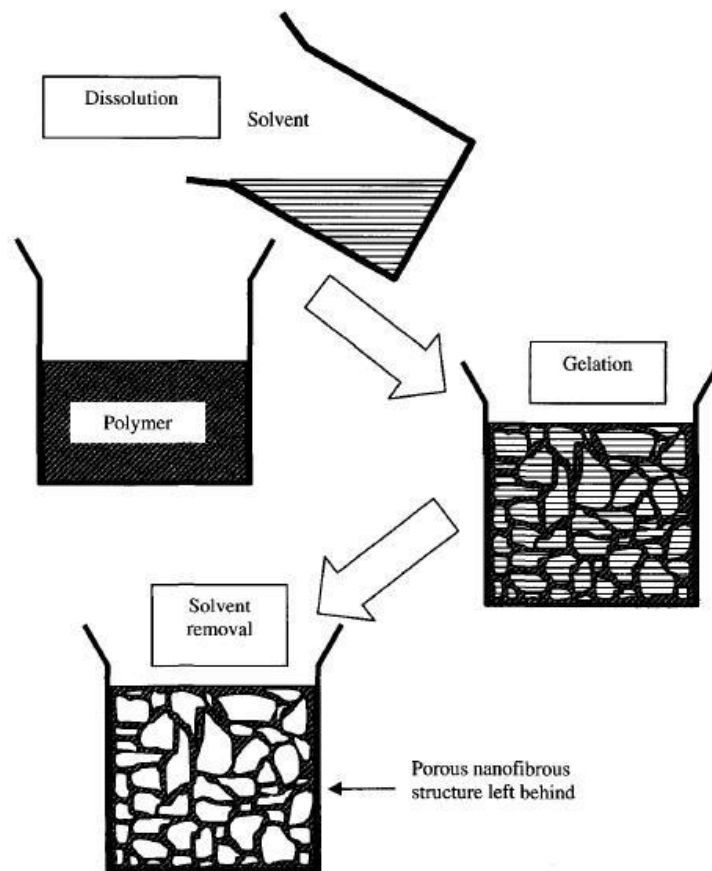


Fig 1.3: Schematic of phase separation process for nanofiber production [1]

1.1.4 Self-Assembly

The prime mechanism of self-assembly for nanofibers is bringing smaller molecules together, which are the building blocks, by intermolecular forces to form a macromolecular nanofiber. For example, many small molecules arrange themselves into concentric patterns due to intermolecular forces. Many number of such concentric macromolecular patterns further arrange themselves in the normal direction to form a nanofiber. [3]

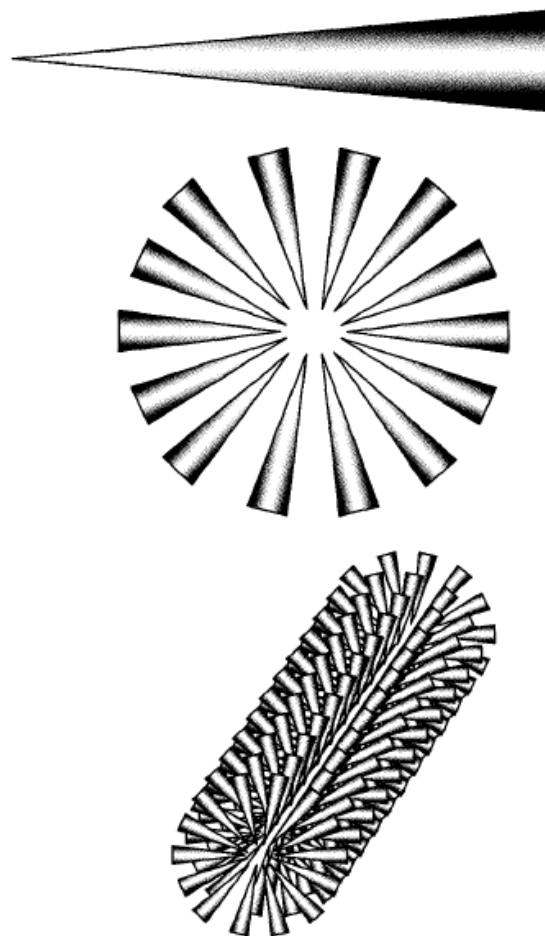


Fig 1.4: Schematic of self-assembly process for nanofiber production [1].

1.1.5 Electrospinning

In electrospinning, a high potential difference is applied between a spinneret, which is mostly a hypodermic needle, and a grounded collector. A polymer solution or fused polymer is pumped out through a syringe and spinneret using a syringe pump. After the buildup of sufficient charge, a jet erupts from a Taylor cone formed at the tip of the spinneret. This jet then travels to the grounded collector, during its flight solvent gets evaporated and fibers of polymer get deposited on the collector. During its flight, there is a charge accumulating in the jet, which exerts a repulsive force within the jet and causes stretching of fibers during its formation which reduces its diameter. Different morphologies can be attained during electrospinning process, ranging from beads, beaded fibers, fibers of different diameters and length to the surface roughness of the fibers depending on the process conditions used. Major factors that affect the morphology include solution parameters and processing parameters. Solution parameters include concentration, molecular weight of polymer, viscosity of solution, surface tension, and electrical conductivity, whereas processing parameters consist of voltage, flow rate, distance between the collector and syringe tip. Apart from these, ambient parameters such as humidity and temperature also have significant effect on the morphology of the fibers.

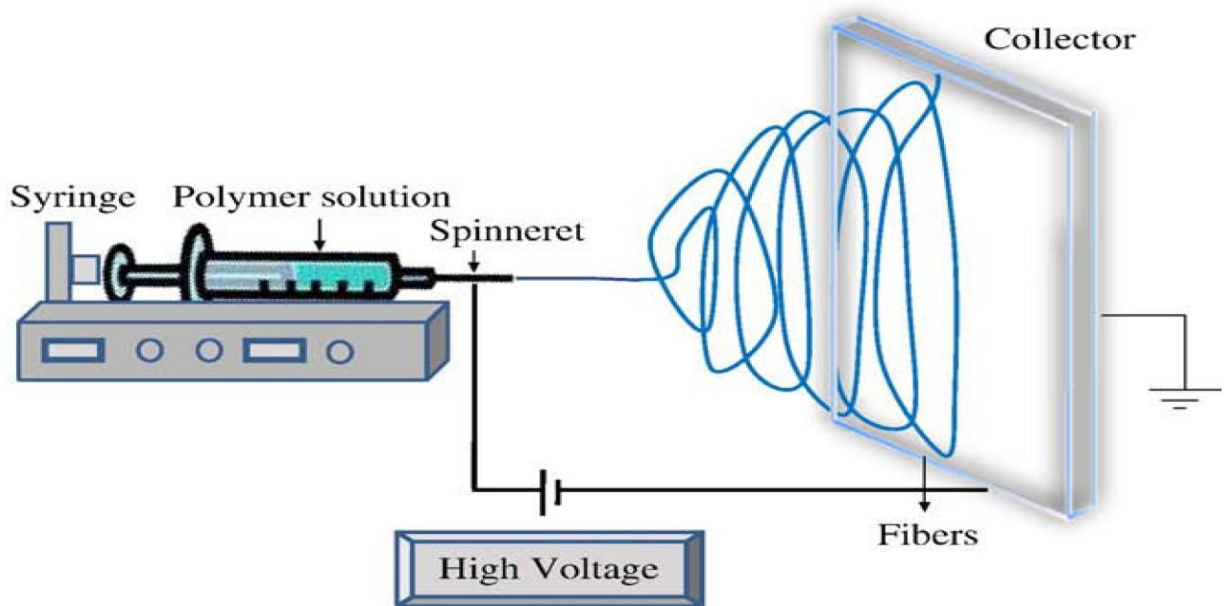


Fig 1.5: Schematic of Electrospinning setup [4]

Factors affecting the morphology of electrospun nanofibers:

Viscosity:

Viscosity plays an important role in determining the fiber morphology. Fiber diameter increases with increase in viscosity of solution. If the viscosity of solution is too high, the solution may solidify at the tip of needle thus clogging the needle. If the viscosity of solution is too low, then it is difficult to obtain smooth and continuous fibers.

Surface tension:

If surface tension is high, solution tends to form spherical droplet to minimize its surface area. This leads to formation of beads after evaporation of solvent. Surface tension can be manipulated by adding surfactants.

Concentration:

Increase in concentration causes an increase in viscosity of solution, thus,

concentration has an indirect influence by means of viscosity as discussed above.

Molecular weight:

For linear chain polymers, increase in molecular weight is caused by increase in chain length of polymer. This increased chain length leads to an increase the chain entanglements and finally the viscosity of solution.

Conductivity:

The charge accumulation on the jet leads to its stretching and bending instabilities which increases the deposition area and leads to formation of fine fibers. More charges can be carried if the conductivity of the jet is increased. The conductivity of the solution can be increased by the addition of ions. Small amounts of salt or polyelectrolytes can be added for this purpose. Conductivity can also be increased by changing the solution pH.

Dielectric Effect of Solvent:

Solutions with higher dielectric property reduce the bead formation and helps to get fine fibers.

Processing Parameters:

Voltage:

Mostly higher voltages cause an increase in the columbic forces which leads to an increase in stretching and formation of fine fibers. But increase in voltage also causes an increase in jet velocity thus a smaller flight which causes increase in the fiber diameter.

Flow Rate:

With increase in flow rate, the drying time for a given volume of solution is decreased; this causes insufficient stretching of fibers and lead to the formation of beaded fibers with larger diameter.

Distance between spinneret and collector:

Distance between spinneret and collector affects flight time and strength of the field. With shorter distance, less flight time is available and causes improper stretching which may result in thick beaded fibers.

Collector:

Conductivity of the collector plays an important role in the process as it dictates the rate of charge dispersion of charge accumulation. Different modes of collecting fibers are being used by using collectors such as flat plate, rotating drum, rotating disk, parallel rods, mesh, grid, rotating rod etc.

Ambient Parameters:

Temperature:

Increase in temperature causes a decreases in viscosity of solution, thus changes in temperature have similar but opposite effects as that of change in viscosity discussed earlier.

Humidity:

Increased humidity causes condensation of water on the cooling jet during the process

of electrospinning. This leads to formation of pores during vaporization of water and solvent.

1.2 Block Copolymers

The polymer formed by polymerization of two or more different types polymeric units is called a Copolymer. When the copolymer is formed by the repeating blocks of the monomer units, it is called a block copolymer. The block copolymer formed by the repeating blocks of two different monomeric units is called diblock copolymer were as those formed repeating blocks of three different monomeric units is called triblock copolymer and those with more than three blocks are called multiblock.

Block copolymers possess a special property of undergoing microphase separation to form periodic nanostructures. This process of phase separation can be understood by the thermodynamic of interaction between the blocks. Since the blocks in a block copolymer are covalently bonded to each other thus they cannot undergo macrophase separation. Thus, due to incompatibility between the blocks, it undergoes microphase separation to form nanometer-sized structures. The extant of incompatibility between the blocks is dictated by the product of degree of polymerization, η and Flory-Huggins parameter, χ . For instance, a diblock copolymer of symmetric composition would undergo a microphase separation only if $\eta\chi$ is greater than 10.5.

Block copolymers are considered as pre-eminent among the category of self-assembling materials because:

- By merely varying the molecular weight, temperature and monomer structure, domains of desired dimensions can be obtained from about 5nm to 50nm.

- Depending upon the molecular weight, the volume fractions of the blocks and the

interaction parameter between the monomer blocks, phase separation may result in four thermodynamically stable state namely lamellae, hexagonally packed cylinders, bicontinuous cubic double gyroid and body-centered cubic arrays of spherical micelles.

➤ By changing one of the blocks, desired properties can be imparted to the system. Thus, block copolymers have an advantage of tailorability in its properties.

➤ Amphiphilic block copolymers may have a number of applications such as Emulsifiers, De Emulsifiers, Defoamers and low-foaming surfactants, Foam stabilizers, in laundry detergents, in dental care products, etc [5].

The ability of block copolymers to form nanostructured arrays via phase separation make them a potential candidate for applications in the fields of data storage, electronics, molecular separation and DNA screening. The phase separated domains can also as a nanoreactor for synthesis of inorganic nanoparticles [6]

One of potential application of block copolymer is in synthesis of nanoporous structures which are formed by selectively removing one of the phase separated domains. These porous polymer materials either in form of films, fibers or some other morphology can have wide application in microfiltration or can be used as templates in electronic industry. [7]

controllable porosity, Large surface area and flexibility in surface functionalization make block copolymer nanofibers a potential candidate for applications in the fields of superhydrophobic surfaces [8], optical and electrical applications [9], biological applications [10], membrane and composite applications [11] and biomedical applications [12]. Bioactive molecules can be immobilized on the functionalized block

copolymers for targeted drug delivery applications.

Bhattacharai, et al. showed that the hydrolytic degradation time of electrospun Poly (*p*-dioxanone-*co*-L-lactide)-*block*-poly(ethylene glycol) was more than that of casted film, it was proposed that this may be due to the autocatalytic degradation in case of casted films. Due to this tunability in the degradation rate, it becomes an attractive candidate in the field of tissue engineering [13]. Synthesis of a pH-responsive block copolymer nanofiber for highly sensitive actuators was carried out by Linge Wang et.al. The polymer used here was a triblock copolymer Poly(methyl methacrylate)-*block*-poly[2-(diethylamino)ethyl methacrylate]-*block*-poly(methyl methacrylate), (PMMA-*b*-PDEA-*b*-PMMA). Here PDEA block acts as a pH-responsive polymer where as PMMA block is a hydrophobic glassy polymer, the process is governed by the rate of diffusion, so the large surface area provided by nanofiber was highly beneficial. It was found that after annealing the fibers in solvent vapor, it can give sustained volume expansion and contraction which is necessary for the pH sensing application [14]. Chi-Ching kuo et al. showed the photoluminescence effect of electrospun Poly[2,7-(9,9dihexylfluorene)]-*block*-Poly(methyl methacrylate) (PF-*b*-PMMA) block copolymer. They also showed the effect of solvent and their combination on the absorption and photoluminescence spectrum of the fibers. The solvents used here were DMF, THF, and DMF: THF (1:1). Upon electrospinning, non-porous fibers with surface roughness were obtained. This surface roughness was caused by the aggregation of PF segment since DMF is a poor solvent for PF. Those PF domains showed dot-like (5–10 nm) structures, line-like (10–20 nm) structures and ellipse-like (25–50 nm) structures with different concentrations of DMF in DMF/THF mixture (0, 10 & 50%). This caused the absorption peak maximum to increase from 370nm to 375nm and emission maxima to increase from 418nm to 437nm as the DMF content

increased from 0% to 100% respectively. Thus, it was shown that by varying the solvent, light absorption and photoluminescence can be tuned [15]. Minglin Ma showed the effect of cylindrical confinement on phase separation of electrospun block copolymer nanofiber. Here they have used out a coaxial electrospinning technique to form a shell of random copolymer, poly(methylmethacrylate-*co*-methacrylic acid)(P(MMA-*ran*-MAA)) outside the core of a block copolymer. When poly(styrene-*block*-isoprene-*block*-styrene) (SIS) was used as a material for core, a concentric layer structure was formed as a core inside the shell of P(MMA-*ran*-MAA). This was caused the curving of the lamellar phase due to the fiber confinement with outermost layer of core being isoprene by the effect of surface tension. When poly(styrene-*block*-isoprene) was used as a core material, Spherical isoprene microdomains dispersed in the styrene matrix were formed. Decorating one of the blocks with nanoparticles or carbon nanotubes can be an effective way to disperse these nano-objects in electrospun fibers in a well-controlled manner or Selective functionalization or removal of one of the blocks may lead to highly functional or porous fibers [16]. Thus, the block copolymer derived electrospun nanofibers can have highly versatile applications.

1.3 Objective and Layout

In this thesis, we have worked on three distinct problems. First two problems deal with the synthesis of porous nanofibers from block copolymers. Basic technique remains same in both the cases. This includes the formation of nanofibers of desired morphology as well as generation of pores within the fibers. PS-*b*-PMMA and PAN-*b*-PMMA block copolymers were used as polymer precursors. The mechanism behind this entire process is explained in detail in chapters 2 and 3. The mesoporous nanofibers thus obtained can have possible application for having a coating of desired

wettability, as an absorbent or a carrier for catalyst. The porous fibers obtained in the first step were further pyrolyzed to convert the polymer derived fibers into the carbon fibers. The porous carbon fibers thus obtained can have a possible application as an anode material for lithium ion battery. In third problem, we worked on the data based modeling of PAN fibers. To the best of our knowledge there is no other technique available to predict the morphology (diameter, length and bead density) of the fibers. Here we use the artificial neural network which is a form of surrogate mode to predict the morphology of the fibers. A detailed description of the technique is given in chapter 4.

Polymers Used:

PS-*b*-PMMA (polystyrene-*b*-poly (methyl methacrylate))

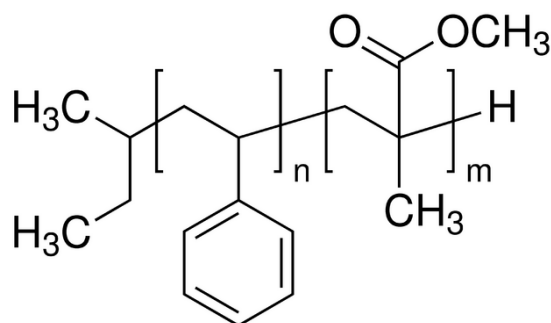


Fig 1.6: Molecular structure of PS-*b*-PMMA

Three block copolymer of different molecular weights were used

Sr No.	Mn for PS (g/mol)	Mn for PMMA (g/mol)	Mw/Mn
1	57,000	25,000	1.07
2	96,500	35,500	1.11
3	280,000	290,000	1.15

Properties: The block copolymer PS-b-PMMA is thermally stable. Two of its blocks have high interaction energy due to which it can easily undergo microphase separation to minimize its free energy. PS is chemically inert and resistant to most acids. When polystyrene is subjected to UV radiation, it becomes stable. PMMA is a tough and rigid polymer but sensitive to UV radiations, thus it can be easily degraded by UV exposure and later can be etched out using an etchant.

PAN-b-PMMA (polyacrylonitrile-b-poly (methyl methacrylate))

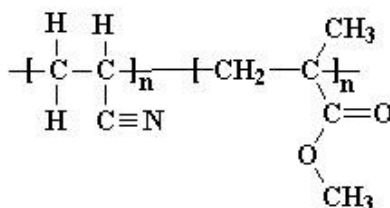


Fig 1.7: Molecular structure of PAN-b-PMMA

Mn for PAN: 1,100 g/mol

Mn for PMMA: 11,000 g/mol

Mw/Mn: 1.2

Properties: PAN is known to be a very good precursor for the production of carbon nanofibers. To synthesize porous carbon fibers we need a sacrificial block which can be easily removed. PMMA seem to be very attractive candidate to act as a sacrificial material due to above-mentioned properties of PMMA. Thus PAN-b-PMMA seems to be a most suitable material for the production of porous carbon fibers. Porosity in pristine fibers was achieved in the manner as described in the case of PS-b-PMMA. Porous fibers thus obtained were stabilized by heating at some suitable conditions to

Chapter 2

Mesoporous Nanofibers Prepared by Electrospinning of PS-b-PMMA

An effective means to obtain mesopores in electrospun block copolymer nanofibers is presented. A solution of block copolymer PS-b-PMMA in an organic solvent was electrospun to obtain polymer nanofibers. A comprehensive study of the effect of molecular weight and concentration of polymer on the morphology of fibers and beads was carried out. The electrospinning parameters were fine-tuned to obtain fibers with negligible beads. Effect of two solvents with different volatilities and their varying composition on fiber morphology was also studied, which showed a drastic change in morphology. The nanofibers thus obtained were thermally annealed to undergo a microphase separation. The phase with PMMA rich domains was selectively etched out using a weak acid as an etchant. The effect of temperature and time of annealing on the morphology of fibers was also studied. The samples were further structurally characterized using SEM, FESEM and FTIR. Wettability studies of as-spun and porous fibers with different morphologies was carried out using goniometer, which revealed that fiber morphology has significant effect on the contact angle.

2.1 Materials

PS-b-PMMA block copolymers with three different molecular weights, PS(57k)-b-PMMA(25k)(Mw/Mn=1.07), PS(96.5k)-b-PMMA(35.5k) (Mw/Mn=1.11), & PS(280k)-b-PMMA(290k) (Mw/Mn=1.15), were purchased from Polymer Source and

used directly without any processing. N,N-Dimethylformamide (DMF) and Tetrahydrofuran (THF) were purchased from S D Fine-Chem Limited (SDFCL), India. Reagent, Acetic acid (99.7%) was purchased from Alfa Aesar, India. Deionized water was obtained from millipore water purification system.

2.2 Method

2.2.1 Preparation of solution

Different solutions were prepared by varying the concentration of polymer, to study the effect of molecular weight and concentration.

Sr No.	Polymer	Solvent	Concentration (wt%)
1	PS(57k)-b-PMMA(25k)	DMF	18
2	PS(57k)-b-PMMA(25k)	DMF	20
3	PS(96.5k)-b-PMMA(35.5k)	DMF	14
4	PS(96.5k)-b-PMMA(35.5k)	DMF	16
5	PS(280k)-b-PMMA(290k)	DMF	3
6	PS(280k)-b-PMMA(290k)	DMF	4
7	PS(280k)-b-PMMA(290k)	DMF	5

Table 2.1: Solutions prepared for electrospinning

Apart from the above mentioned solutions, five more solutions of PS(280k)-b-PMMA(290k) with different solvent (DMF:THF) ratios of mixing were prepared.

These include,

Sr No.	Polymer	Solvent (DMF:THF)	Concentration (wt%)
1	PS(280k)-b-PMMA(290k)	1:0	5
2	PS(280k)-b-PMMA(290k)	2:1	5
3	PS(280k)-b-PMMA(290k)	1:1	5
4	PS(280k)-b-PMMA(290k)	1:2	5
5	PS(280k)-b-PMMA(290k)	0:1	5

Table 2.2: Solutions prepared by varying (DMF:THF) ratio

2.2.2 Electrospinning

The Electrospinning process was carried out with a horizontal arrangement of the setup at room temperature. Silicon wafer mounted on aluminum foil using conductive carbon tape was used as a collector. Table 2.3 shows the variations in the parameters carried out so as to get fine fibers with minimum number of beads.

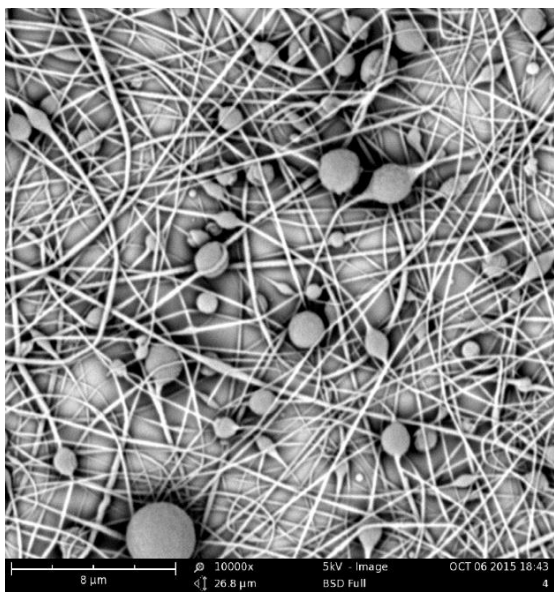
Variation in parameters			
Parameters	PS(57k)-b-PMMA(25k)	PS(96.5k)-b-PMMA(35.5k)	PS(280k)-b-PMMA(290k)
Flow Rate (µl/min)	1-3	2-5	3-7
Voltage (kV)	8-20	8-20	8-20
Distance (cm)	5-17	5-17	5-17

Table 2.3: Tuning of electrospinning parameters.

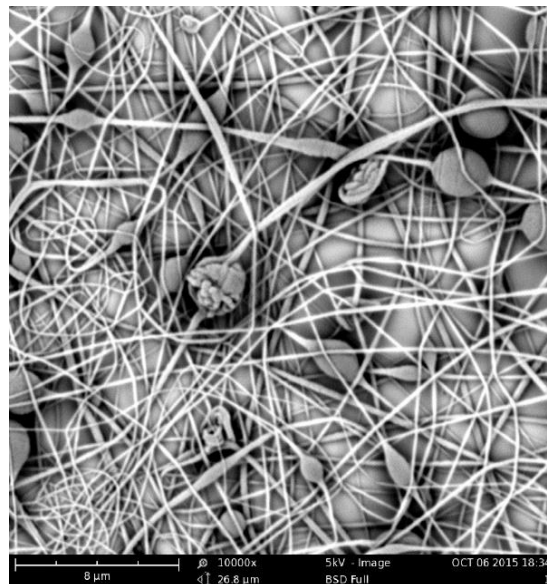
The SEM characterization revealed the morphology of the electrospun fibers and the following parameters are found to be better in terms of minimum beads.

Sr No	Polymer	Concentration (wt%)	Flow rate (µl/min)	Needle gauge	Voltage (kV)	Distance (cm)
1	PS(57k)-b-PMMA(25k)	18	2	22	20	8
2	PS(57k)-b-PMMA(25k)	20	2	22	20	8
3	PS(96.5k)-b-PMMA(35.5)	14	3	22	18	15
4	PS(96.5k)-b-PMMA(35.5)	16	3	22	18	15
5	PS(280k)-b-PMMA(290k)	3	5	22	14	8
6	PS(280k)-b-PMMA(290k)	4	5	22	14	8
7	PS(280k)-b-PMMA(290k)	5	5	22	14	8

Table 2.4: Solutions used to study the effect of molecular weight and concentration.

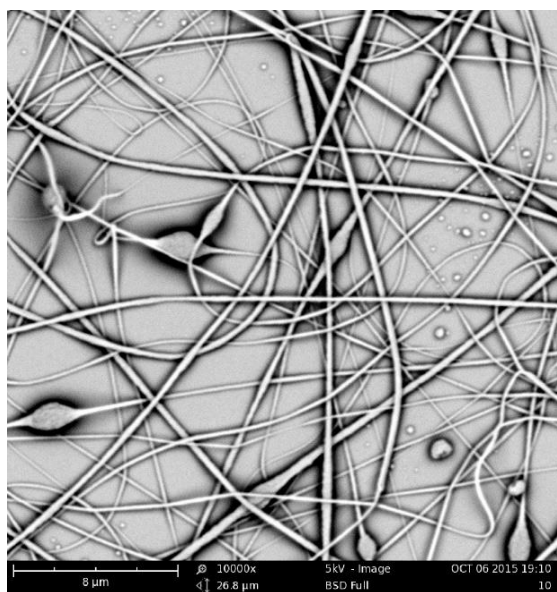


(a)

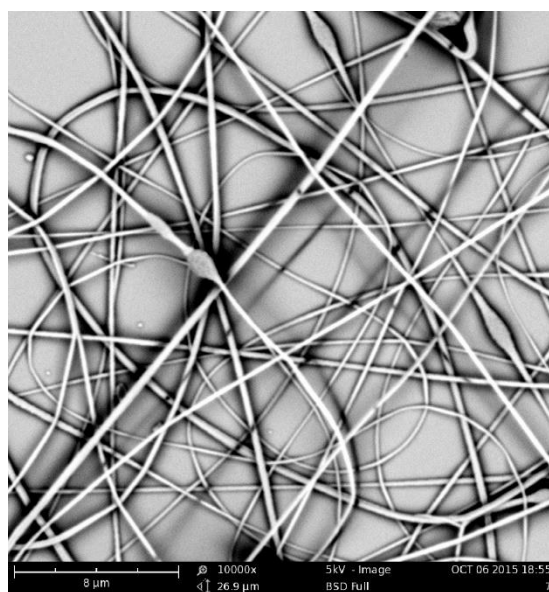


(b)

Fig 2.1: SEM images of PS(57k)-b-PMMA(25k) as-spun nanofiber (a) 18wt%, (b)20wt% in DMF



(a)

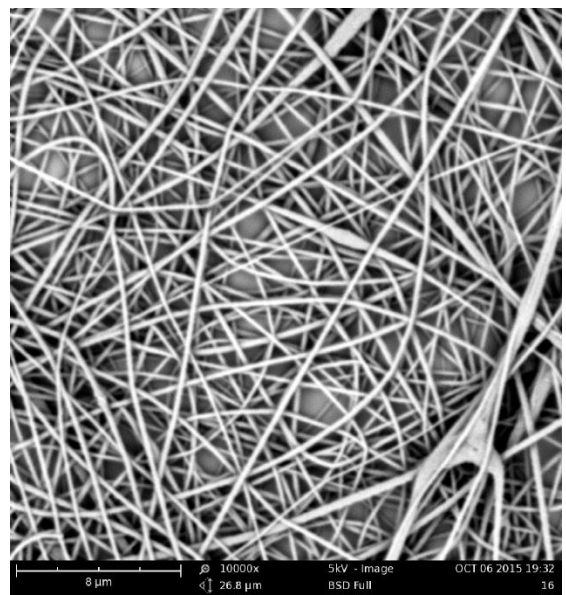


(b)

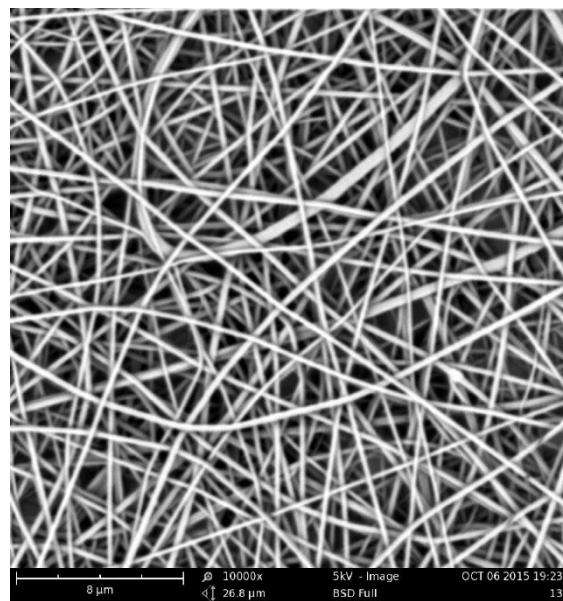
Fig 2.2: SEM images of PS(96.5k)-b-PMMA(35.5k) as-spun nanofiber (a) 14wt%, (b)16wt% in DMF



(a)



(b)



(c)

Fig 2.3: SEM images of PS(280k)-b-PMMA(290k) as-spun nanofiber (a) 3wt%, (b) 4wt%, (c) 5wt% in DMF

2.2.3 Formation of porous PS-b-PMMA fibers

The As-spun fibers thus obtained were thermally annealed which increases chain mobility and assist phase separation. The annealing process was carried out at 165⁰C in vacuum for different time durations varying from 1h to 12 h to find the optimum annealing time (because the morphology of fibers must not be disturbed after thermal treatment). The vacuum was maintained at -500mm Hg during annealing. Vacuum oven was switched on and allowed to reach 165⁰C under vacuum then the as-spun samples were introduced into the oven at elevated temperature. After annealing the samples were brought back to room temperature and were allowed to cool.

The thermal annealed samples were exposed to UV light (365 nm wavelength) for 1 min in a UV chamber. UV light causes cross-linking to Polystyrene phase and at the same time causes degradation of Poly(methyl methacrylate). The degraded PMMA phase was then etched out by immersing the samples in acetic acid and gently agitating for 30 s. Any spent acid was washed away by washing the samples with deionized water for 30 s.

2.3 Characterization and Analysis

2.3.1 Characterization using SEM

The scanning electron microscope (SEM) uses a focused beam of high-energy electrons to generate a variety of signals at the surface of solid specimens. The signals that derive from electron-sample interactions reveal information about the sample

including external morphology (texture), chemical composition, and crystalline structure and orientation of materials making up the sample. [17]

The as-spun samples were gold coated using the sputtering technique to increase their conductivity. These gold-coated samples were then characterized using SEM. A comprehensive analysis of SEM images was carried out to find average bead size, bead size distribution, average fiber diameter, fiber size distribution, the number of beads per unit area (i.e. bead density) and percentage of deposited area occupied by beads. To carry out this analysis, for a particular sample, three images taken at different locations of a sample and analyzed individually. Average bead size was found by manual measurements using MagniSci image analyzing software.

This data was used to find its size distribution. Summing up all such beaded area gives the total area covered by beads. Phase fraction analyzes package was used to find out the total deposited area (i.e., area occupied by both bead and fiber) thus, we can find the percentage of deposited area occupied by beads. Average fiber diameter was found by using Fibermetric application available with Phenom desktop SEM and its size distribution was found using this data.

Results and Discussion:

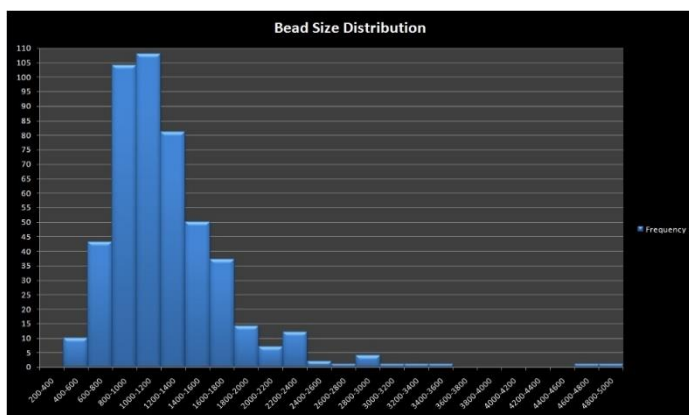
Table 2.5 shows the variation in the number of per 1000 μm^2 of substrate area, average bead diameter, total area occupied by beads per 100 μm^2 of substrate area, average fiber diameter and the percentage of the deposited area occupied by beads with respect to the change in the solution concentration in case of PS(57)-b-PMMA(25).

Tables 2.6 and Table 2.7 show the same variations in case of PS(96.5)-b-PMMA(35.5) and PS(280k)-b-PMMA(290k) respectively.

	18wt%	20wt%
No.of Beads/1000 μm^2	55	28
Avg Bead Diameter	1.25 \pm 0.5 μm	1.74 \pm 0.9 μm
Area occupied by bead per 100 μm^2 Total area	7.8 μm^2	7.94 μm^2
Area of deposition per 100 μm^2	49.17 μm^2	48.48 μm^2
Avg Fiber diameter	259 \pm 63 nm	274 \pm 64 nm
Percentage of deposited area occupied by bead	15.86%	16.38%

Table 2.5: Effect of concentration on the morphology of PS(57k)-b-PMMA(25k) at optimum electrospinning parameters.

Fig 2.4 and Fig 2.5 shows the bead size distribution and fiber size distribution respectively for PS(57k)-b-PMMA(25k).

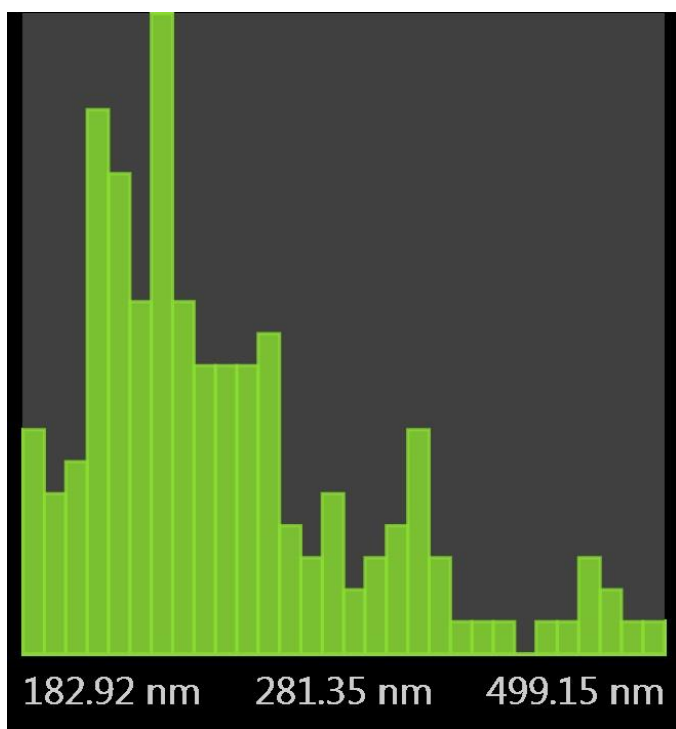


(a)



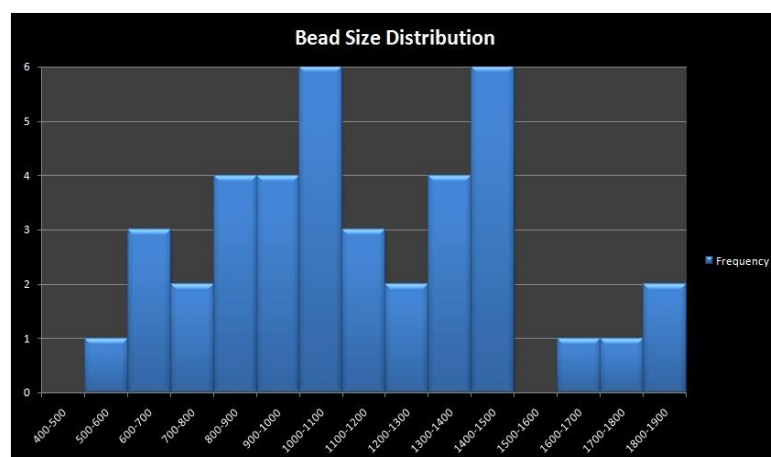
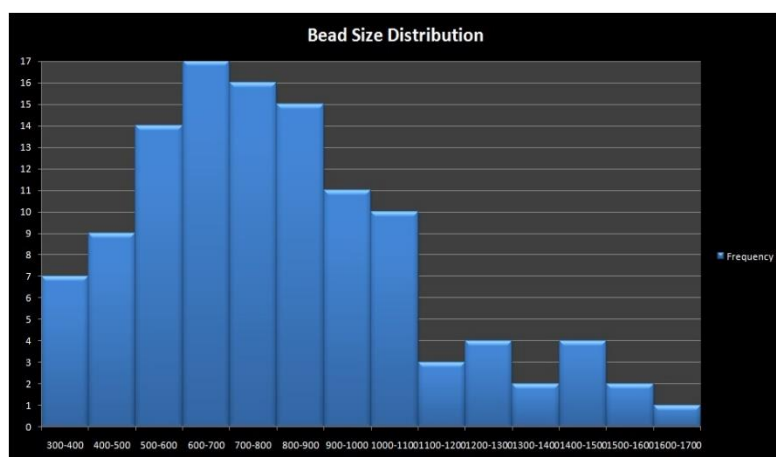
(b)

Fig 2.4: Bead size distribution for (a)18wt% & (b) 20wt% PS(57k)-b-PMMA(25k)



	14wt%	16wt%
No.of Beads/1000 μm^2	13	5
Avg Bead Diameter	857 \pm 31 nm	1110 \pm 42 nm
Area occupied by bead per 100 μm^2 Total area	0.76 μm^2	0.61 μm^2
Area of deposition per 100 μm^2	23.14 μm^2	24.79 μm^2
Avg Fiber diameter	248 \pm 67nm	263 \pm 64nm
Percentage of deposited area occupied by bead	3.28%	2.46%

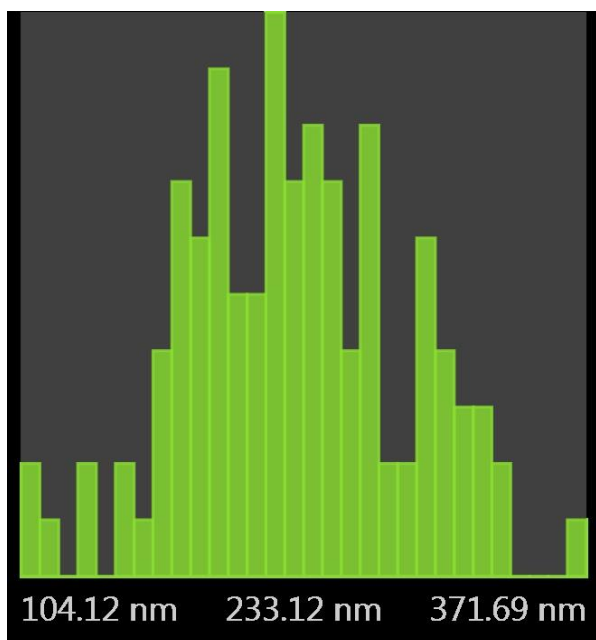
Table 2.6: Effect of concentration on PS(96.5k)-b-PMMA(35.5k) nanofibers.



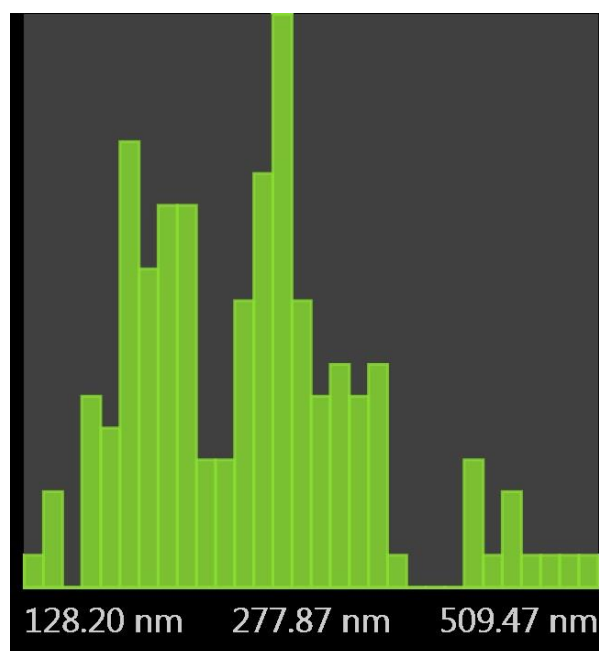
(a)

(b)

Fig 2.6: Bead size distribution for (a) 14wt% & (b) 16wt% PS(96.5k)-b-PMMA(35.5k)



(a)



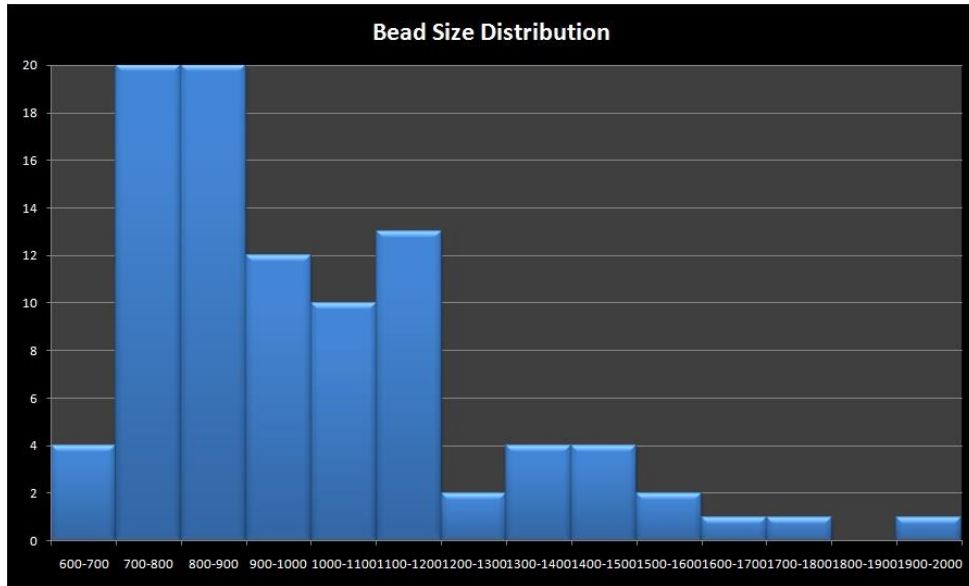
(b)

Fig 2.7: Fiber size distribution for (a)14wt% & (b)16wt% PS(96.5k)-b-PMMA(35.5k)

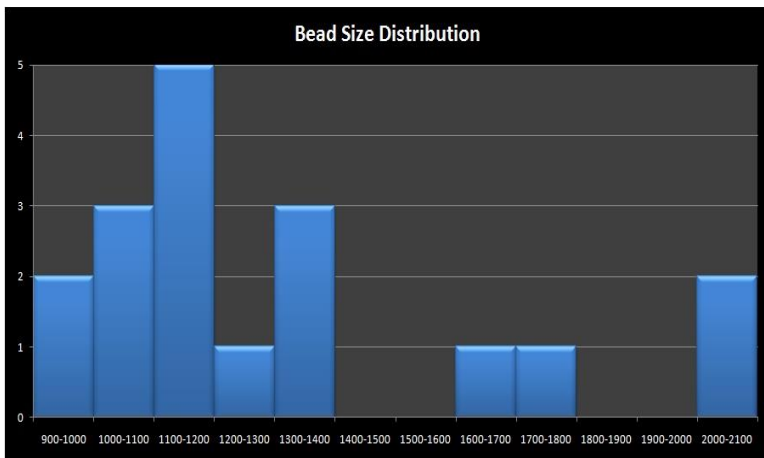
	3wt%	4wt%	5wt%
No.of Beads/1000 μm^2	11	2	~ 0
Avg Bead Diameter	1 ± 0.3 μm	$1.3 \pm 0.3 \mu\text{m}$	$1.23 \pm$ $0.4 \mu\text{m}$
Area occupied by bead per $100 \mu\text{m}^2$ Total area	$0.9 \mu\text{m}^2$	$0.31 \mu\text{m}^2$	$0.04 \mu\text{m}^2$
Area of deposition per 100 μm^2	$67.96 \mu\text{m}^2$	75.22 μm^2	73.68 μm^2

Avg Fiber diameter	263±56nm	332±82nm	336± 73 nm
Percentage of deposited area occupied by bead	1.32%	0.41%	0.065%

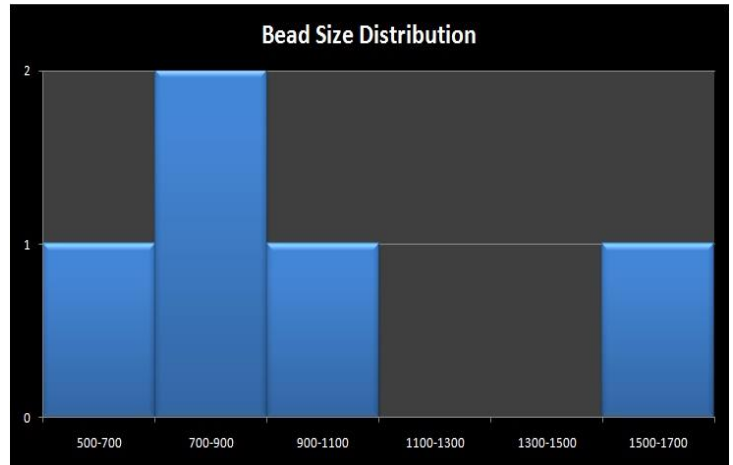
Table 2.7: Effect of concentration on the morphology of PS(280k)-b-PMMA(290k) at optimum electrospinning parameters.



(a)

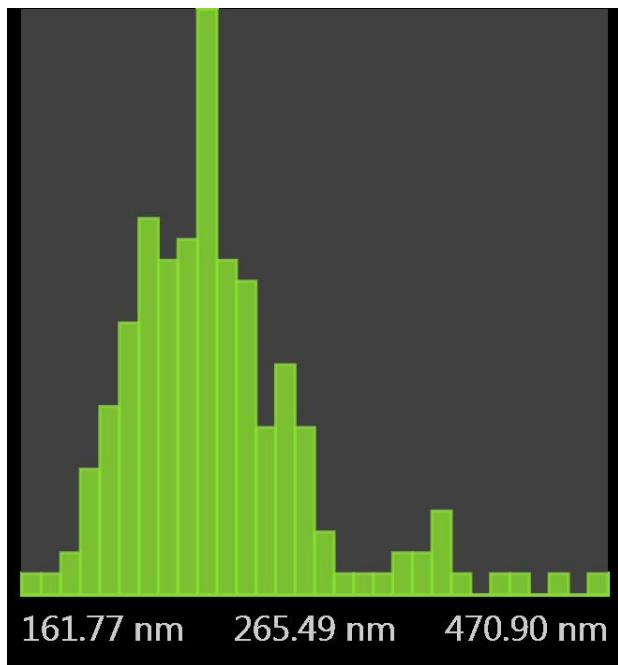


(b)

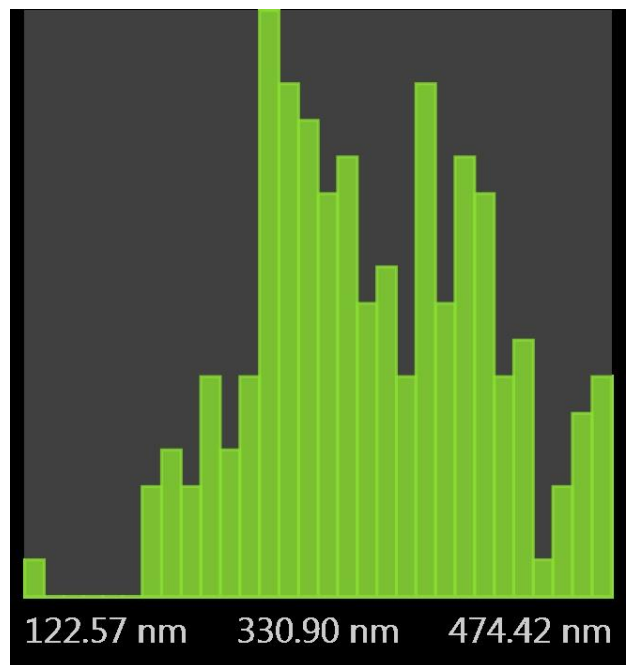


(c)

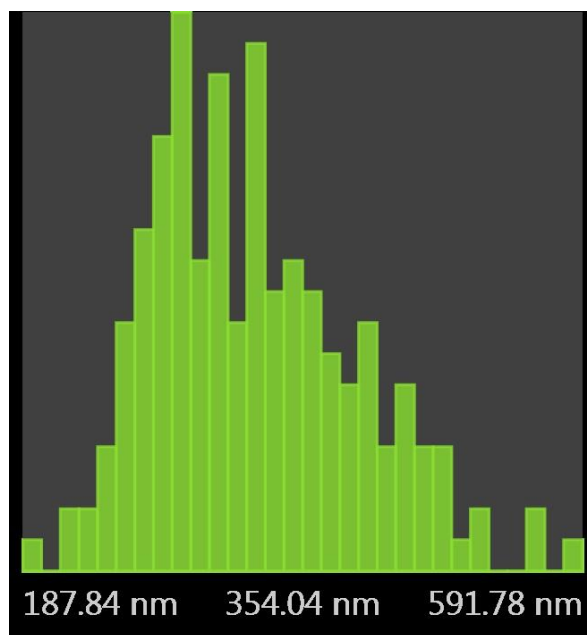
Fig 2.8: Bead size distribution for(a) 3wt%,(b) 4wt% & (c) 5wt% PS(280k)-b-PMMA(290k)



(a)



(b)



(c)

Fig 2.9: Fiber size distribution for (a)3wt%, (b)4wt% & (c)5wt% PS(280k)-b-PMMA(290k)

It is observed that,

- The number of beads decreases with increase in concentration in all the cases.
- The diameter of bead increases with increase in concentration in case of PS-b-PMMA(57k-25k) & PS-b-PMMA(96.5k-35.5k) and first it increases as concentration changes from 3% to 4% and then decreases as concentration changes from 4% to 5% for PS-b-PMMA(280k-290k).
- Percentage of deposited area occupied by beads increases with increases in concentration in case of PS-b-PMMA(57k-25k) and it decreases with increases in concentration in case of PS-b-PMMA(96.5k-35.5k) & PS-b-PMMA(280k-290k)
- The diameter of fiber increases with increase in concentration in all three cases.
- The number of beads per unit area decreases with increase in molecular wt.
- Percentage of deposited area occupied by beads decreases with increase in molecular wt.

The effect of thermal annealing time on the morphology for fibers also studied and it was found that at 165°C, 12 h of annealing caused complete distortion of fiber morphology. After annealing at 165°C for 6 h the morphology was partially retained and after annealing at 165°C for 1h, the morphology was completely retained.

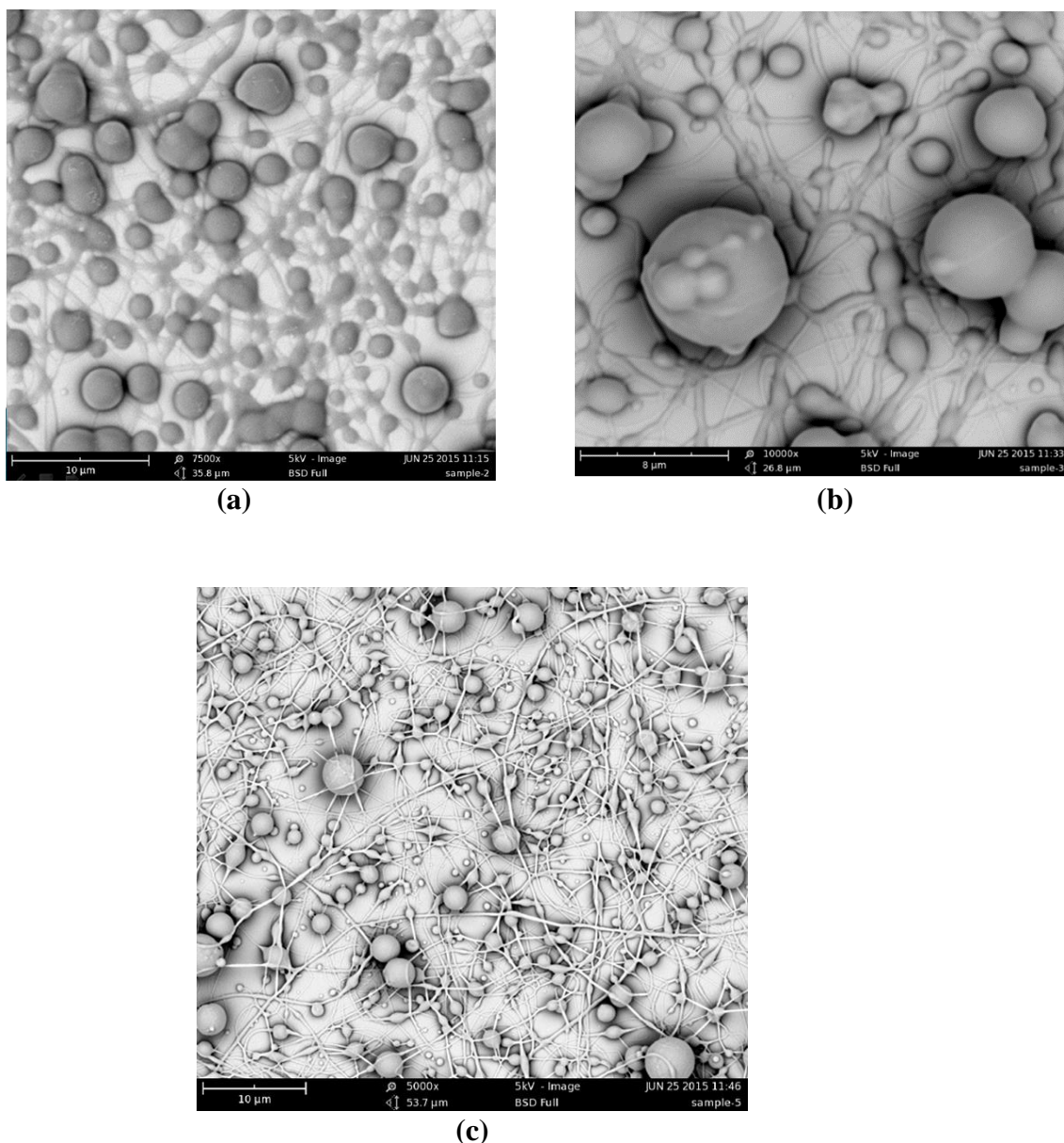


Fig 2.8: Effect of thermal annealing on morphology of PS(57k)-b-PMMA(25k) fibers. Fibers gets completely melted when annealed at 165 °C for 12hr (a), partial melting takes place when annealed at 165 °C for 6 hr (b), fiber morphology is retained when annealed for 1hr at 165 °C.

Later, the samples were exposed to UV light which causes crosslinking of PS phase and at the same time degradation of PMMA phase which was later etched out using acetic acid leading to porosity in fibers.

The effect of solvent on fiber morphology was also studied. Different solvents have different level of electrospinnability [18]. Thus it is important to select such a solvent that has good solubility as well as spinnability. The factors which decide the

spinnability of the solution includes molecular weight, solution viscosity, surface tension, solution conductivity, dielectric property of Solvent [1]. The solvent used here is a mixture of two solvents, DMF and THF, with their varying concentrations. A gradual change in the morphology of fibers can be observed as the concentration of THF changes from 0% THF to 100% THF.

It is observed that when THF was used as a solvent, the as-spun fibers obtained were highly porous. This can be attributed to the high volatility and rapid vaporization of THF during electrospinning [19]. But it has been observed that the annealing treatment causes closing of majority of the pores, thus the pore density was reduced as compared to pristine fibers.

2.3.2 FTIR

Method:

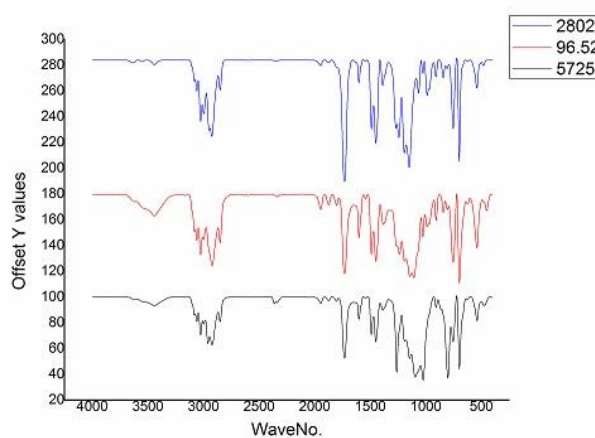
FTIR is a tool that is used to identify the functional groups of a compound.

Some of the infrared radiation is absorbed by the sample and some of it is passed through(transmitted). The resulting spectrum represents the molecular absorption and transmission, creating a molecular fingerprint of the sample. Like a fingerprint, no two unique molecular structures produce the same infrared spectrum. An FTIR (Bruker, Tensor 37), equipped with the Universal ATR Sampling Accessory was used to obtain spectra in the 500 - 4000 cm^{-1} region.

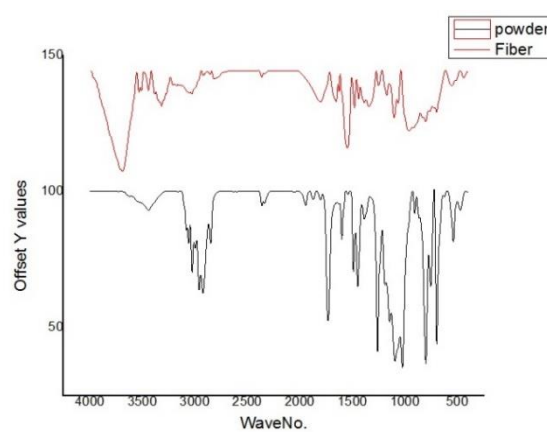
FTIR studies were carried out for polymer powder of all three molecular weight of PS-b-PMMA and of the fibers obtained at their respective optimized electrospinning conditions for 20 wt% PS(57k)-b-PMMA(25k), 16wt% PS(96.5k)-b-PMMA(35.5k), 5% wt PS(280k)-b-PMMA(290k).

Results:

Fig 2.27 shows an FTIR spectrum for the PS-b-PMMA powder and fibers. These results show the various groups present in the fibers which can be correlated to the groups present in the block copolymer. The three sharp peaks obtained between 1450-1600 cm^{-1} corresponds to the three conjugated C=C double present in the benzene ring of polystyrene block. Peaks just above 3000 cm^{-1} correspond to stretching vibration of sp² hybridized C-H bonds in polystyrene block. Peaks just below 3000 cm^{-1} correspond to stretching vibration of sp³ hybridized C-H bonds in both polystyrene and poly(methyl methacrylate) blocks. Peaks just above 1400 cm^{-1} correspond to C-H bending vibrations in both the blocks. The peak between 1000-1100 cm^{-1} corresponds to C-O bond of sp³ hybridized carbon and that between 1200-1300 cm^{-1} corresponds to C-O bond of sp² hybridized carbon of PMMA block. The peak between 1700-1750 cm^{-1} corresponds to the stretching vibration of C=O bond in PMMA block.



(a)



(b)

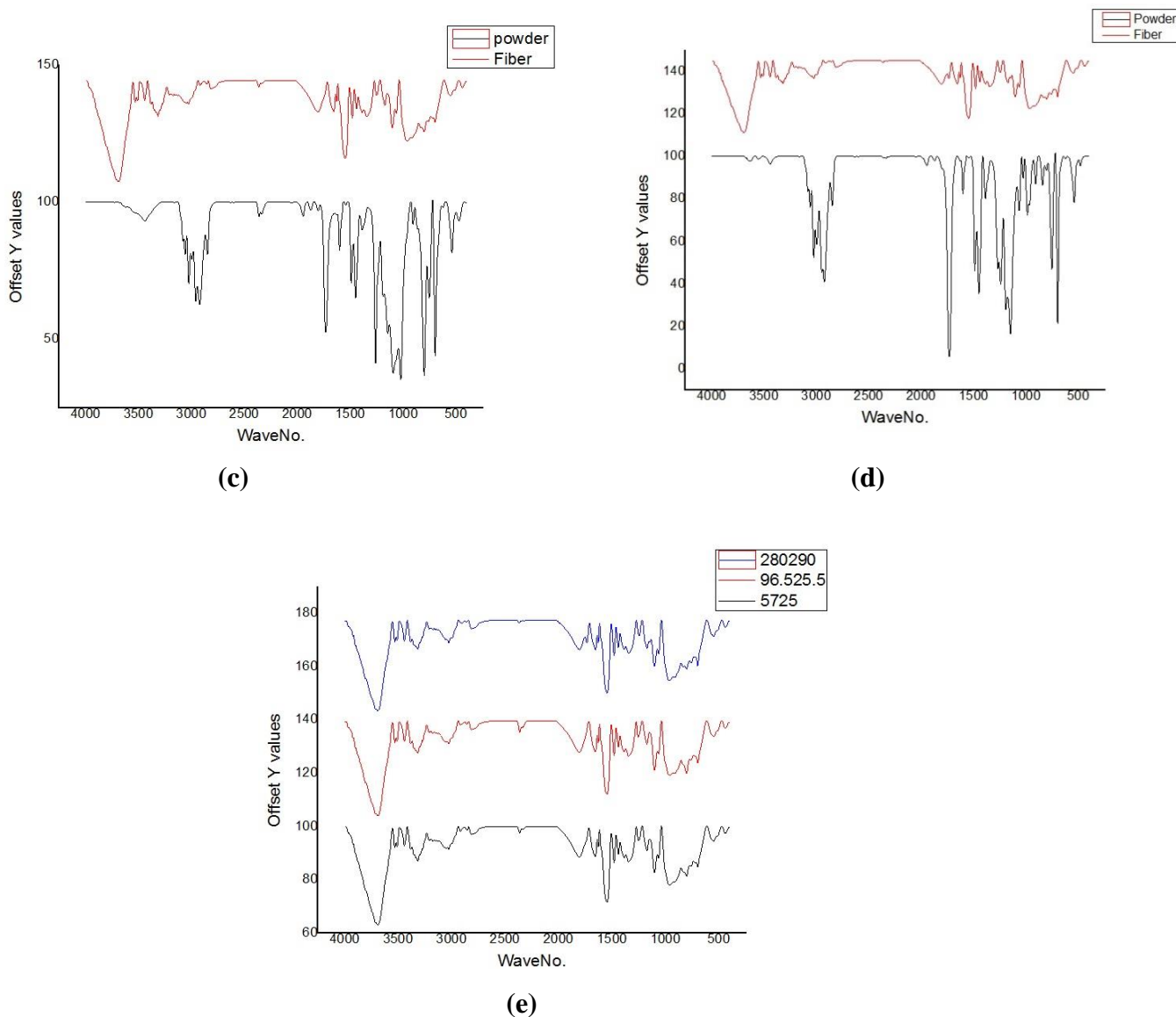


Fig 2.9: (a) compares the FTIR spectra of polymer powders of all three molecular weights, (b) compares the FTIR spectra of powder & fibers of PS(57k)-b-PMMA(25k), (c) compares the FTIR spectra of powder & fibers of PS(96.5k)-b-PMMA(35.5k), (d) compares the FTIR spectra of powder & fibers of PS(280k)-b-PMMA(290k), (e) compares the FTIR spectra of polymer fibers of all three molecular weights.

2.3.3 Wettability Studies

Wettability is the property of a solid surface to allow a fluid to spread on or adhere to

the surface. Wettability of a surface is studied by measuring the contact angle made by a fluid, mostly water when placed on it. The angle subtended by the tangent to the liquid droplet and the solid surface is called contact angle.

Hydrophobic surface – A Surface which repels water is termed as a hydrophobic surface. Hydrophobic surfaces have a contact angle greater than 90° .

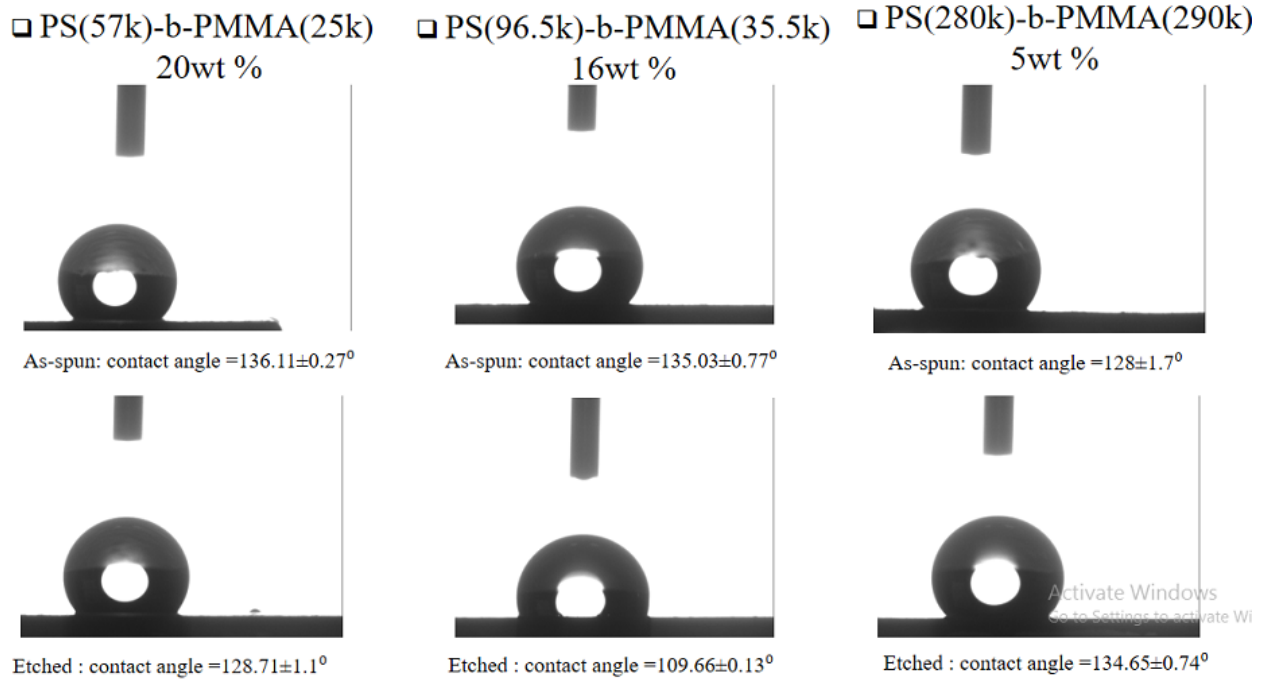
Hydrophilic surface - A Surface which adheres water is termed as a hydrophilic surface. Hydrophilic surfaces have a contact angle less than 90° .

Superhydrophobic – Surfaces having contact angle more than 150° are called superhydrophobic surfaces.

Contact angle studies were carried out for both as-spun and porous fibers of all three molecular weights, electrospun at their respective optimized electrospinning parameters. These include 20 wt% PS(57k)-b-PMMA(25k), 16wt% PS(96.5k)-b-PMMA(35.5k) and 5% wt PS(280k)-b-PMMA(290k). These results were also compared with a pure bead morphology, which was obtained by electrospinning 5 wt% PS(57k)-b-PMMA(25k) at 3 μ l/min with a potential difference of 20kV and tip to collector distance of 15cm using a 22g needle and its respected porous beads.

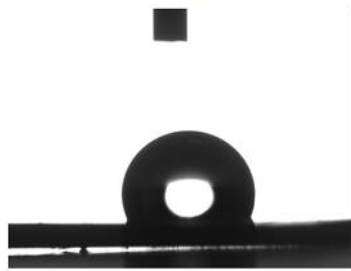
Contact angle studies were also carried out for spin-coated films of above-mentioned solutions, for both pristine and their respective porous spin coated films. The spin coating was carried out at 3000rpm for 1min and the porosity was generated the same procedure as in the case of electrospun fibers.

Results: It was observed the fibers show higher contact angle than their respective spin coated films for all the molecular weights of PS-b-PMMA. Also for each of the molecular wt. porous fibers, beads, and films, contact of porous was less than their pristine counterparts. Thus, a vast range of wettability can be obtained, from slightly hydrophilic to highly hydrophobic with different morphologies.

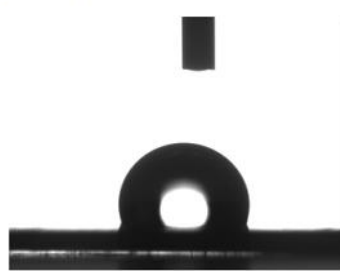


a

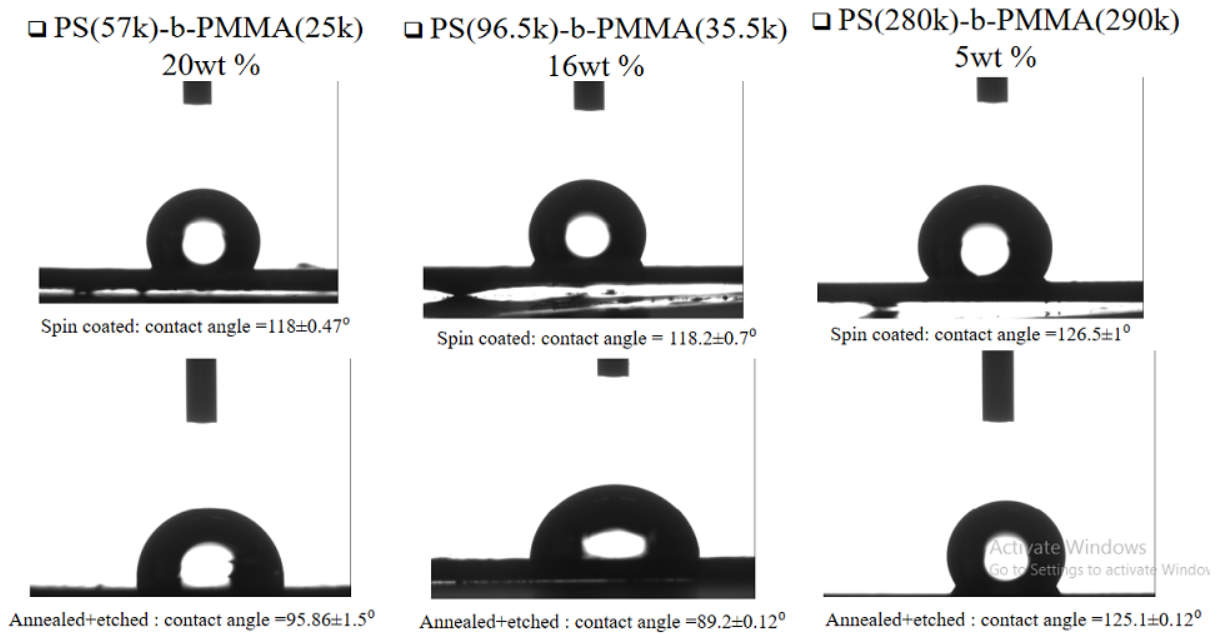
□ **Beads: PS(57k)-b-PMMA(25k) 5wt%**



As-spun: contact angle = $111 \pm 2.4^\circ$



Annealed+etched : contact angle = $104.75 \pm 3.75^\circ$



c

Fig 2.10: (a) Goniometer images for measurement of contact angle for fiber and beaded fiber morphology of all three molecular weights for as-spun and porous fibers.(b) Show the measurement of contact angle for beads of PS(57k)-b-PMMA(25k) for as-spun and porous beads.(c) Show the measurement of contact angle for spin coated films of all three molecular weights for as-coated and porous films.

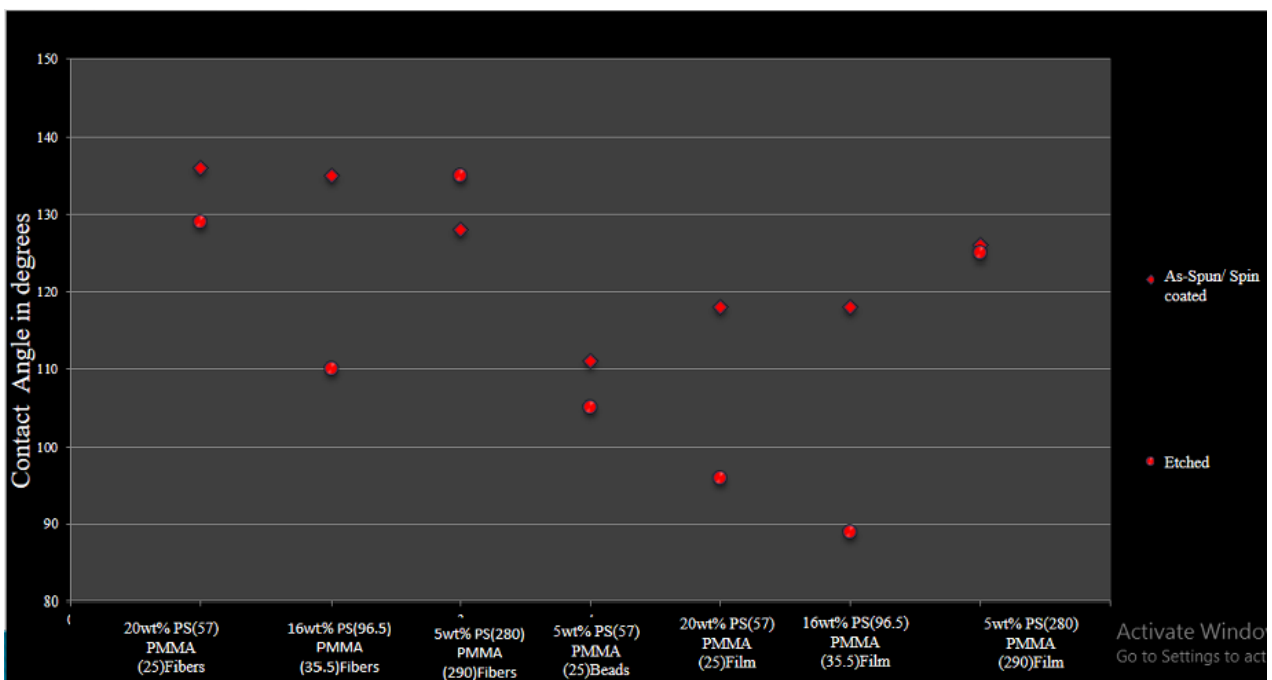


Fig 2.11: Comparative study of contact angles of all the morphologies

Chapter 3

PAN-b-PMMA Derived Electrospun Nanofibers

3.1 Materials

PAN(1.1k)-b-PMMA(11k) ($M_w/M_n=1.20$) block copolymer was purchased from Polymer Source and used directly without any processing. PAN(150k) was purchased from Sigma-Aldrich. N,N-Dimethylformamide (DMF) was purchased from S D Fine-Chem Limited (SDFCL), India. Reagent, Acetic acid (99.7%) was purchased from Alfa Aesar, India. Deionized water was obtained from millipore water purification system.

3.2 Method

3.2.1 Preparation of solution

Three solutions of PAN with concentrations of 7wt%, 8wt%, and 9wt% were prepared in DMF. Each of these solutions was then blended with a solution of 12wt% PAN-b-PMMA in DMF in ratio 1:1 (V/V), thus forming three blended solutions for electrospinning.

3.2.2 Electrospinning

The Electrospinning was carried out using a silicon wafer as a substrate mounted on aluminum foil using conductive carbon tape was used as a collector. The Flow rate was varied from 5 μ l/min to 10 μ l/min, applied potential difference was varied from 10kV to 18kV and tip to collector distance was varied from 10cm to 12cm for each of the

solution blends so as to get fine beadless fibers.

Electrospinning parameters were fixed to following values (optimum parameters) after SEM characterization which gave fine beadless fibers: A blend of 8wt% PAN in DMF and 12wt% PAN-b-PMMA in DMF (1:1) (V/V), flow rate of 10 μ l/min, applied potential difference of 18kV and tip to collector distance 12cm with 22g needle as spinneret.

3.2.3 Formation of porous PAN-b-PMMA fibers

The As-spun fibers thus obtained were thermally annealed which increases chain mobility and assist phase separation. The annealing process was carried out at 180^oC in vacuum for 12h. The vacuum was maintained at -500mm Hg during annealing.

The thermal samples were than exposed to UV (365 nm wavelength) for 1 min in a UV chamber. UV light causes cross-linking in PAN phase and degradation in Poly(methyl methacrylate) phase. The degraded PMMA phase was then etched out by immersing the samples in acetic acid and gently agitating for 30s. Any spent acid was washed out using DI water. FESEM images reveal the formation of mesopores onto the surface of nanofibers.

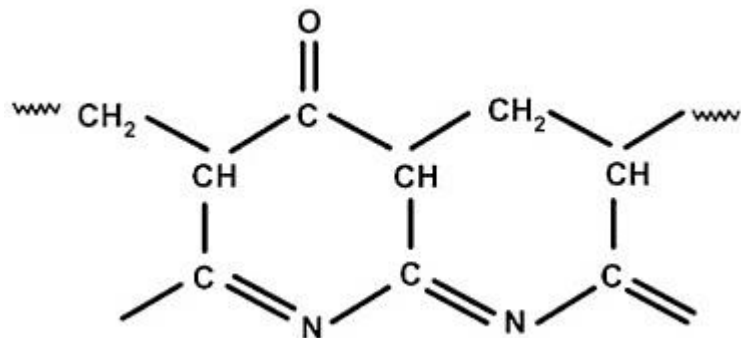


Fig 3.3: Ladder structure of PAN [21]

Cyclization reaction starts at 180 °C and proceeds slowly till 220 °C and later proceeds very rapidly till 289 °C [21]. On further increase in temperature, there is an increase in the number of the carbonyl group and there is a degradation in the ladder structure of polymer [22], [23]. This rate of degradation is maximum at about 380 °C [24]. Thus, the temperature selected for stabilization process was 250 °C and the stabilization process was carried out for 1h in an oven. Carbonization was carried out in a high-temperature furnace. For carbonization, the stabilized fibers were first heated from room temperature to 350 °C at a heating rate of 3 °C/min and held at 350 °C for half an hour later the temperature was increased from 350 °C to 900 °C by heating at the rate 5 °C/min and held at 900 °C for 1hr. It was observed that the average fiber diameter decreases from ~235 nm to ~137nm after carbonization.

3.3 Characterization and Analysis

3.3.1 FTIR

An FTIR (Bruker, Tensor 37), equipped with the Universal ATR Sampling Accessory was used to obtain spectra in the 500 - 4000 cm^{-1} region. FTIR studies were carried out for as-spun PAN/PAN-b-PMMA fibers and the for the fibers after pyrolysis.

Results:

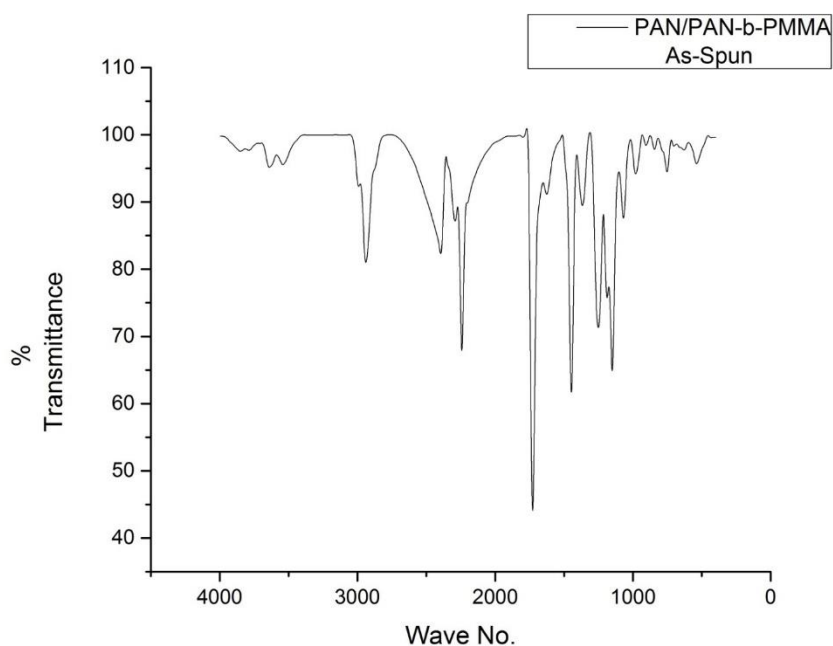


Fig 3.4: FTIR of as-spun PAN/PAN-b-PMMA nanofibers.

Fig 3.6 shows an FTIR spectrum for the as-spun PAN/PAN-b-PMMA fibers. These results show the various groups present in the fibers which can be correlated to the groups present in the block copolymer and homopolymer. Peak 2939 cm^{-1} (Just below 3000 cm^{-1}) corresponds to sp^3 hybridized C-H bonds of both PAN and PMMA blocks. The sharp peak at 2241 cm^{-1} corresponds to nitrile group of PAN. The sharp peak at 1710 cm^{-1} corresponds to the carbonyl group of PMMA block. The peak 1448 cm^{-1} corresponds to CH bending vibration of R_2CH_2 & R_3CH groups. The band of peaks between $1000\text{-}1300\text{ cm}^{-1}$ corresponds to sp^2 & sp^3 hybridized CO bonds.

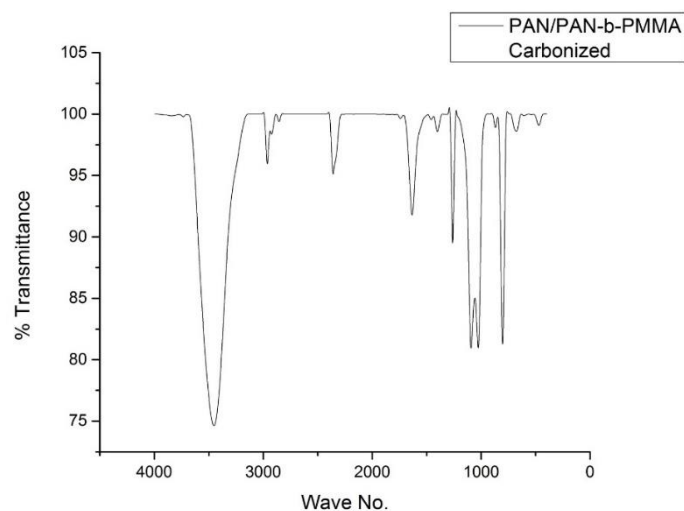


Fig 3.5: FTIR of pyrolyzed PAN/PAN-b-PMMA nanofibers.

Fig 3.7 shows an FTIR spectrum for the pyrolyzed PAN/PAN-b-PMMA fibers. A sharp peak at 3452 cm^{-1} corresponds to NH group stretching vibration which is formed during the pyrolysis process. Peak 2962 cm^{-1} corresponds to sp^3 hybridized C-H bond. The peak at 1634 cm^{-1} corresponds to C=N bond. It is to be noted that the strong absorption peak located in the 2241 cm^{-1} in as-spun fibers, which is characteristic of a nitrile group, completely disappears upon pyrolysis.

3.3.2 Raman spectroscopy

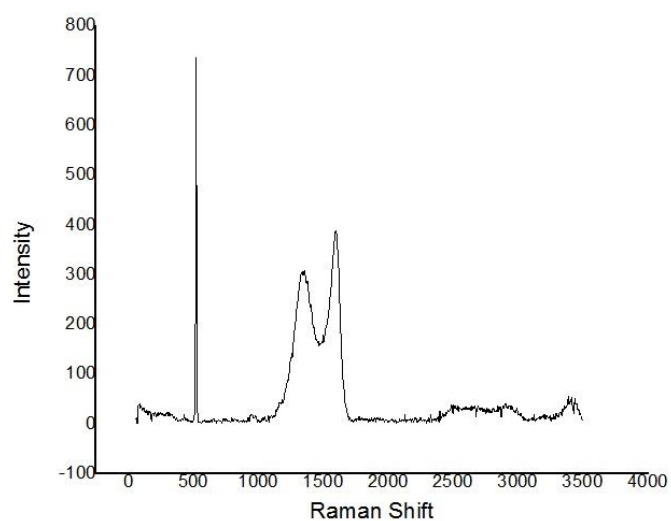


Fig 3.6: Raman spectroscopy image of pyrolyzed PAN/PAN-b-PMMA nanofibers.

Raman spectroscopy is used to study the chemical composition of material. Raman spectroscopy studies the inelastic scattering of light. It was observed by Dr. C.V Raman in 1928. It studies the inelastic scattering of light. When a monochromatic radiation of frequency ν_0 is allowed to interact with molecules and the scattered radiation is found to contain only original frequency ν_0 (Rayleigh scattering) as well as a pairs of new frequencies of the type $(\nu_0 \pm \nu_M)$. The new frequencies are referred to as Raman bands and together they constitute a Raman spectrum. Raman bands are always characterized by the frequency shift $|\nu - \nu_0| = \nu_M$.

Raman spectroscopy was carried out for the structural characterization of carbonized samples. The sharp peak at about 519 cm^{-1} is that of the Si wafer which was used as a substrate. The broad peaks found at around 1330 cm^{-1} (D band), 1599 cm^{-1} (G band) and between $2500\text{-}3300 \text{ cm}^{-1}$ (G' band), revealed the formation amorphous carbons with nano graphitic structures [25]. The ratio of intensities (I_d/I_g) was found to 1.262. Crystallite size (L_a) was then calculated using the formula, $L_a = 4.4/(I_d/I_g) \text{ nm}$ which comes out to be 4.4 nm.

3.3.3 Transmission electron microscopy (TEM)

TEM is an electron microscopy technique in which the electrons transmitted through the ultrathin samples are used for the imaging purpose. As TEM uses electrons for imaging purposes, resolution as high as 0.2 nm, which is typical spacing between the atoms, can be achieved due to small de Broglie wavelength of electrons.

TEM characterization was carried out for the carbonized pristine fibers and the carbon fibers obtained after treatment. TEM images of pristine carbonized fibers reveal that the d spacing between the layers is $\sim 3.7 \text{ \AA}$.

It was observed that there was a complete loss in crystallinity in the carbon fibers obtained after treatment of as-spun fibers. The same can be inferred from the electron diffraction images.

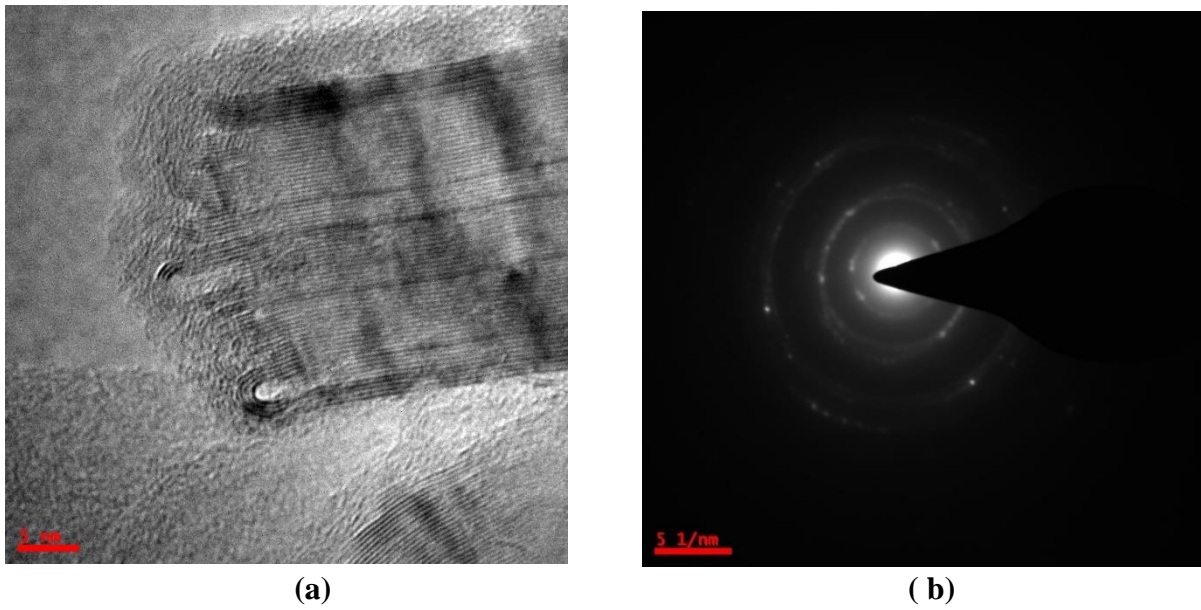


Fig 3.7: (a)TEM image and (b) electron diffraction image of pyrolyzed as-spun fibers.

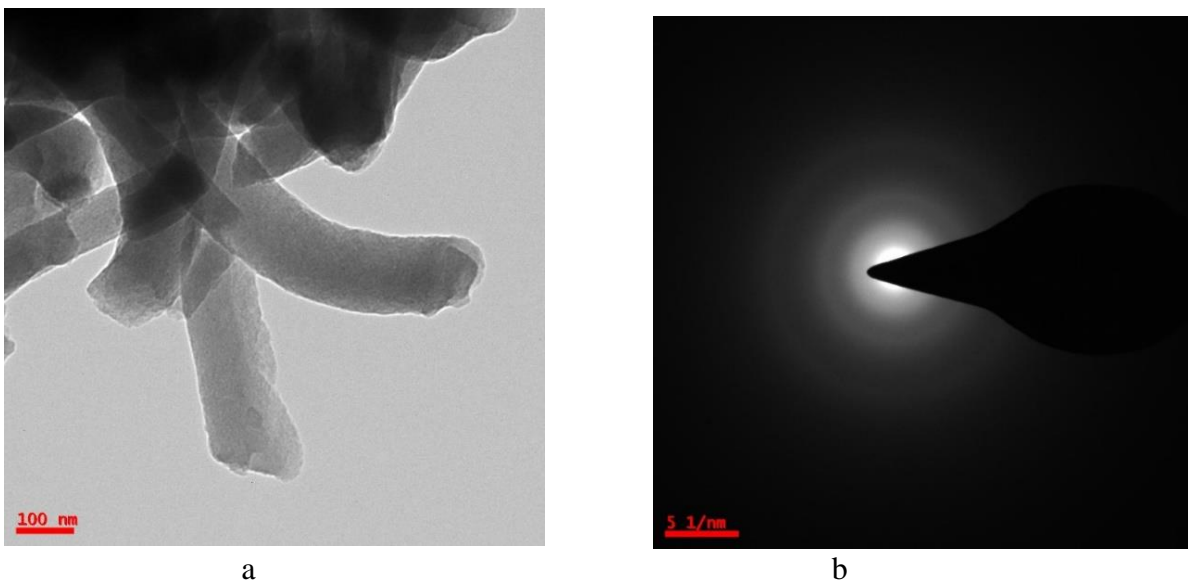


Fig 3.8: (a)TEM image and (b) electron diffraction image of pyrolyzed and etched fibers.

Chapter 4

Data Based Modeling of Electrospun PAN Nanofibers

4.1 Materials

PAN(150k) was purchased from Sigma Aldrich. N,N-Dimethylformamide (DMF) was purchased from S D Fine-Chem Limited (SDFCL), India.

4.2 Experimentation

Electrospinning was carried out to collect the data which was later used for modeling purpose. Electrospinning data was collected by varying the following parameters; the concentration of PAN was varied from 3 g/ml to 8 g/ml with interval of 1 g/ml, needle size was varied from 18G to 26G with interval of 2G, flow rate was varied from 2 μ L/min to 10 μ L/min with the interval of 2 μ L/min, the distance between spinneret and collector was varied from 5cm to 15 cm with interval of 1cm and the applied potential difference was varied from 8kV to 15kV with an interval of 1kV.

4.3 Characterization

The fibers were characterized using an optical microscope. Depending upon the morphology the fibers were classified as beads, fibers or beaded fibers. Depending upon the size, the fibers with length more than 20 μ m were classified as long fibers and those with size less than 20 μ m were classified as short fibers. Fiber diameter was found using ImageJ software, to calculate the Avg. fiber diameter, diameter was

sampled at ten different locations and was averaged to get the Avg. fiber diameter.

Inputs									
Sample No.	Concentration	Needle gauge	Flowrate(microliter/min)	Distance from collector plate(cm)	Voltage(KV)	Remark	Diameter	Morphology	Size
1	3	18	2	5	8		1671.8576	1	-
2	3	20	6	12	14		1508.774	1	-
3	3	20	10	10	12		1336.8167	1	-
4	3	22	2	13	12		608.6988	2	2
5	3	22	6	7	11		498.405	3	2
6	3	22	8	14	11		627.7886	3	1
7	3	24	4	9	14		623.5034	3	1
8	3	24	4	11	10		570.7656	3	1

Sample No.	1	2	3	4	5	6	7	8	9	10
Spot										
1	962.724	881.705	1204.996	677.134	485.547	743.046	604.628	608.438	529.931	647.694
2	1861.119	1415.617	976.974	618.253	457.778	645.682	613.169	569.184	485.944	596.934
3	1249.687	1829.286	1501.201	544.851	500.394	589.547	647.693	595.965	500.394	570.537
4	1204.996	1265.143	1728.781	568.021	546.747	465.496	626.223	569.184	539.745	555.484
5	2641.846	1804.565	858.374	671.995	490.677	677.773	739.083	533.191	518.17	639.313
6	1619.662	2543.904	1396.264	594.125	500.394	648.361	492.244	545.688	653.319	541.437
7	3492.98	1280.413	1406.435	638.597	468.179	623.835	718.736	502.698	569.185	555.484
8	1147.722	1852.513	1165.645	559.566	379.062	671.348	726.466	538.94	557.906	466.53
9	1619.662	1223.139	1772.448	621.051	589.14	591.748	557.906	616.302	579.913	481.164
10	918.178	991.455	1357.049	593.395	566.132	621.05	508.886	628.066	632.041	499.455
Avg Diameter	1671.858	1508.774	1336.817	608.6988	498.405	627.7886	623.5034	570.7656	556.6548	555.4032
Corrected sample stan	819.2437	499.1633	295.2012	45.23937	59.81138	72.71313	87.40328	40.96465	54.13259	61.6869

Morphology Notation	
Bead	1
Fibre	2
Beaded Fibre	3
Size Notation	
Broken	1
Long	2

Number of Sample points = 100

Fig 4.1: An illustration of format of collected data

Chapter 5

Summary and Future Work

In chapter 2 we have shown the successful optimization of the electrospinning parameters and studied the effect of solvent, polymer concentration, polymer molecular weight and electrospinning parameters on the fiber morphology. We have also optimized the thermal conditions to assist phase separation and at the same time retain the fiber morphology. Thus the porous nanofibers were produced by selective etching which was characterized by FESEM. FTIR studies of powder and fiber samples confirmed the presence of same functional groups and also gave an insight into the effect of electrospinning on the stretching of bonds. Contact angle studies showed the wide range of wettability properties, from slight hydrophilic to highly hydrophobic, that can be obtained depending upon the morphology. The mesoporous fibers thus obtained can have versatile applications such as coatings for surfaces to obtain desired wettability, a carrier for catalyst, filtration media and for adsorption purposes.

Chapter 3 first explains the tuning of the concentration of PAN/ PAN-b-PMMA blend and optimization of electrospinning parameters to obtain fine beadless fibers. As-spun fibers were then allowed to undergo a phase separation assisted by thermal annealing followed by a UV exposure which causes degradation of PMMA block and finally etching out the degraded block using a weak acid and washing with DI water. The mesoporous fibers thus obtained were characterized by FESEM. FTIR spectroscopy was used to confirm the presence of functional groups. Pristine and porous fibers were then pyrolyzed after stabilization to form mesoporous carbon fibers with yield of about

35%. RAMAN spectroscopy and TEM was used to study the crystallinity of carbon fibers. The mesoporous carbon fibers thus obtained can have a potential application as an adsorbent and as an anode material for lithium ion batteries.

Currently the only way to understand the morphology of electrospun fibers is by experimentation. In chapter 4 we have shown the data based modeling method to predict the morphology of electrospun PAN fibers. The input parameters to our model are polymer concentration, needle size, distance between spinneret and collector, flow rate of solution and applied potential difference. The model thus obtain is able to predict the fiber length, fiber diameter and its morphology. Thus this model can largely reduce the burden of experimentation for the production of electrospun nanofibers.

References

- [1] K. F.-E. T.-C. L. & Z. M. Seeram Ramakrishna, *An Introduction Electrospinning and Nanofibers.*, Ton Tuck Link, Singapore: World Scientific Publishing Co. Pte. Ltd., 2005.
- [2] K. Vibha, M. Sergio, J. Lee, N. Huy, M. Manuel and Y. Joo, "Confined assembly in coaxially electrospun block copolymer fibers.," *Advanced Materials*, vol. 18, no. 24, pp. 3299-3303, 2006.
- [3] J. D. B. E. & S. S. I. Hartgerink, " Self-assembly and mineralization of peptide-amphiphile nanofibers," *Science*, vol. 294, no. 5547, pp. 1684-1688, 2001.
- [4] X. C. Ning Zhu, "Biofabrication of Tissue Scaffolds," in *Advances in Biomaterials Science and Biomedical Applications*'.
- [5] B. L. Paschalis Alexandridis, *Amphiphilic Block Copolymers self assembly and applications*, Amsterdam: ELSEVIER SCIENCE B.V., 2000.
- [6] I. W. Hamley, "Nanostructure fabrication using block copolymers. Nanotechnology," *Nanotechnology*, vol. 14, no. 10, pp. 39-54, 2003.
- [7] G. t. B. Wendy van Zoelen, "Thin films of complexed block copolymers," *Soft Matter*, vol. 5, no. 8, pp. 1568-1582, 2009.
- [8] Y. C. C. Y. K. C. C. T. S. H. K. T. & C. W. C. Chiu, "Synthesis, Morphology, and Sensory Applications of Multifunctional Rod–Coil–Coil Triblock Copolymers and Their Electrospun Nanofibers.," *ACS applied materials & interfaces*, vol. 4, no. 7, pp. 3387-3395, 2012.
- [9] M. J. & M. A. M. Fasolka, "Block copolymer thin films: physics and applications 1," *Annual Review of Materials Research*, vol. 31, no. 1, pp. 323-355, 2001.
- [10] A. H. B. M. Y. & S. Ş. Allı, "Synthesis, characterization and surface properties of amphiphilic polystyrene-b-polypropylene glycol block copolymers," *European Polymer Journal*, vol. 42, no. 4, pp. 740-750, 2006.
- [11] X. W. Z. Y. Z. & W. Y. Yao, "Energy-saving, responsive membranes with sharp selectivity assembled from micellar nanofibers of amphiphilic block copolymers," *Journal of Materials Chemistry*, vol. 1, no. 24, pp. 7100-7110., 2013.
- [12] D. H. B. S. & C. B. Liang, "Functional electrospun nanofibrous scaffolds for biomedical applications.," *Advanced drug delivery reviews*, vol. 59, no. 14, pp. 1392-1412, 2007.
- [13] N. e. a. Bhattarai, "Biodegradable Electrospun Mat: Novel Block Copolymer of," *Journal of Polymer Science*, vol. 41, no. 16, p. 1955–1964, 2003.
- [14] P. D. T. Linge Wang, "Electrospinning pH-Responsive Block Copolymer Nanofibers," *Advanced Materials*, vol. 19, p. 3544–3548, 2007.
- [15] Y.-C. T. Chi-Ching Kuo, "Novel Luminescent Electrospun Fibers Prepared From Conjugated Rod–Coil Block Copolymer of Poly[2,7-(9,9-dihexylfluorene)]-block-Poly(methyl methacrylate)," *Macromol. Rapid Commun*, vol. 29, p. 1711–1715, 2008.
- [16] V. K. Minglin Ma, "Electrospun Polymer Nanofibers with Internal Periodic Structure Obtained by Microphase Separation of Cylindrically Confined Block Copolymers," *Nano Lett*, vol. 6, no. 12, pp. 2969-2972, 2006.
- [17] "Geochemical Instrumentation and Analysis," [Online]. Available: http://serc.carleton.edu/research_education/geochemsheets/techniques/SEM.html.
- [18] W. H. S. J. L. W. M. N. C. P. P. K. R. R. P. S. Teeradech Jarusuwannapooma, "Effect of solvents on electro-spinnability of polystyrene solutions and morphological appearance of resulting electrospun polystyrene fibers," *European Polymer Journal*, p. 409–421, March 2005.
- [19] B. D. J. Y. a. Y. H. Jinyou Lin, "Direct Fabrication of Highly Nanoporous," *ACS Appl. Mater. Interfaces.*, vol. VOL. 2, p. 521–528, 2010.
- [20] A. I. A. M. M.S.A. Rahaman, "A review of heat treatment on polyacrylonitrile fiber," *Polymer*

- Degradation and Stability*, pp. 1421-1432, 2007.
- [21] I. A. David LIB, "Influence of the thermostabilization process," *J Membr Sci*, pp. 213(1-2):285-91, 2002.
- [22] E. M. D. J. Fitzer, "The Influence of Oxygen on the Chemical Reactions During Stabilization of PAN as Carbon Fiber Precursor," *Carbon*, pp. 63-69, 1975.
- [23] O. P. M. L. M. Bahl, "Characterization of Oxidized PAN Fibers," *Carbon*, p. 417 – 423, 1974.
- [24] K. C.-C. Y. W.-T. C. Tse-Nao, "The effect of Stabilization of PAN- Based Carbon Films," *Carbon*, p. 583 – 590, 1993.
- [25] S.-J. Byun and H. Lim, "Graphenes converted from polymers.," *j.Phys. Chem. Lett.*, vol. 2, p. 493–497, 2011.